Master in Chemical Engineering

# *Sustainable Production of Hydrogen Peroxide using Seawater and Solar Energy*

## Master dissertation

of

**Rita Amaral Borges**

**Developed within the course of dissertation**

held in

**Laboratory of Separation and Reaction Engineering - Laboratory of Catalysis and Materials**

SRE CM
*ASSOCIATE LABORATORY*
LABORATORY OF SEPARATION AND REACTION ENGINEERING
LABORATORY OF CATALYSIS AND MATERIALS

Supervisors:

**Doctor Maria J. Sampaio**

**Professor Cláudia G. Silva**

**Professor Joaquim L. Faria**

U.PORTO
FEUP FACULDADE DE ENGENHARIA
UNIVERSIDADE DO PORTO

DEPARTAMENTO DE
ENGENHARIA QUÍMICA

**July 2022**

# Acknowledgments

The commitment and effort made for the fulfillment of this dissertation would not be enough without the support and encouragement of whom I am grateful.

Doctor Maria J. Sampaio, my supervisor, deserves recognition for her constant support, esteem, teaching, and advice both within and beyond the laboratory.

Special appreciation to Professor Cláudia G. Silva, and Professor Joaquim L. Faria, for their mentorship and knowledge sharing.

Thank you to Doctor Marta Pedrosa and Doctor Yaidelin Manrique, members of LSRE-LCM, for their time and support in producing the catalyst immobilization and acquiring SEM pictures.

To my laboratory colleagues, particularly Zuzana Vilamová and André T. Pinto, I'm thankful for their care, empathy, and advice.

My heartfelt gratitude goes to my parents, Leandro, and Eugénia Borges, as well as my sister, Filipa Borges, for their love and unwavering support. Without you, I could not have accomplished everything I have.

To my boyfriend, Tiago Antunes, thank you for always looking out for me, pushing me to be better and achieve greater things.

To my friends who have stood by me throughout the years, thank you for your friendship and support.

This work was financially supported by LA/P/0045/2020 (ALiCE), UIDB/50020/2020 and UIDP/50020/2020 (LSRE-LCM), funded by national funds through FCT/MCTES (PIDDAC), and by NORTE-01-0145-FEDER- 000071 (PORTUGAL2020).

# Abstract

Several serious issues must be addressed all over the world. Poverty, hunger, pollution, climate change, and access to clean and cheap energy are just a few that require immediate attention. Some of the factors are the increasing cost of oil barrels and, eventually, the demise of fossil fuels; a rise in per capita electricity consumption; and an increase in global population, particularly in less developed places. A step towards resolving these issues would be to develop a system for producing an alternative fuel that is entirely sustainable and easy to store. As an added benefit, that can be converted into electricity via complementary technologies.

Hydrogen peroxide is used in various applications, including metal mining and processing, such as uranium extraction and purification. It is also employed in manufacturing stain-free detergents and degradation of components as a water treatment method. It has disinfecting qualities, which are highly valued in the pharmaceutical industry. It could also be used in a one-compartment fuel cell to generate electricity, making it a suitable energy carrier alternative to oil or hydrogen.

Semiconductor photocatalysis has been found as a potential technology to produce hydrogen peroxide and to use it directly as a solar liquid fuel. The key benefits of this process are the use of water as a solvent, the potential of employing biomass derivatives as sacrificial agents, and, ideally, the use of metal-free photocatalysts activated by visible light. Graphitic carbon nitride, a visible-light-responsive material composed entirely of Earth-abundant components such as carbon, nitrogen, and hydrogen, is considered a sustainable catalyst.

Furthermore, two additional benefits can favor this process, namely, the use of seawater as a hydrogen source, which avoids potable water consumption and the possibility of catalyst immobilization, allowing for its simple reuse and possible application in continuous flow systems.

This study has demonstrated that heterogeneous photocatalysis can produce hydrogen peroxide under visible light irradiation using biomass derivatives (*e.g.*, saccharides) as sacrificial agents, seawater as a solvent, and a metal-free catalyst (graphitic carbon nitride). The same scenario was accomplished by using the photocatalyst immobilized in two different supports, which constituted the main novelty of this work, as well as the application of biomass and seawater hydrogen peroxide production.

It is crucial to note that this technology enables on-site manufacture of this alternative fuel and, when combined with a fuel cell, can potentially allow on-site generation of electricity. As a result, it possesses the main features to be considered a promising technology that can help alleviate one of the world's most serious challenges.

**Keywords:** Hydrogen Peroxide, Photocatalysis, Biomass, Seawater, Graphitic Carbon Nitride

# Resumo

Globalmente, há várias questões sérias devem ser abordadas. Pobreza, fome, poluição, alterações climáticas, e acesso a energia limpa e barata são apenas algumas que requerem atenção imediata. Alguns dos fatores são o custo crescente dos barris de petróleo e, eventualmente, o término dos combustíveis fósseis; um aumento do consumo de eletricidade per capita; e um aumento da população global, particularmente em locais menos desenvolvidos. Um passo para a resolução destas questões seria desenvolver um sistema de produção de um combustível alternativo inteiramente sustentável e fácil de armazenar. Como um benefício adicional, que este possa ser convertido em eletricidade através de tecnologias complementares.

O peróxido de hidrogénio é utilizado em várias aplicações, incluindo a extração e processamento de metais, tais como a extração e purificação de urânio. É também utilizado no fabrico de detergentes anti manchas e na degradação de componentes como método de tratamento de águas. Possui qualidades desinfetantes, que são distintamente valorizadas na indústria farmacêutica. Pode também ser utilizado numa célula de combustível de um compartimento para gerar eletricidade, tornando-o uma alternativa energética adequada ao petróleo ou hidrogénio.

A fotocatálise com a aplicação de catalisadores semicondutores, foi encontrada como uma tecnologia potencial para produzir peróxido de hidrogénio e para o utilizar diretamente como combustível líquido solar. Os principais benefícios deste processo são a utilização de água como solvente, a potencial integração de derivados de biomassa como agentes de sacrifício e, idealmente, a utilização de fotocatalisadores isentos de metal ativados pela luz visível. O nitreto de carbono grafítico, um material estimulado pela luz visível composto inteiramente de componentes abundantes da Terra, tais como carbono, azoto e hidrogénio, é considerado um catalisador sustentável.

Além disso, dois benefícios adicionais podem favorecer este processo, nomeadamente, a utilização da água do mar como fonte de hidrogénio, que evita o consumo de água potável, e a possibilidade de imobilização do catalisador, permitindo a sua simples reutilização e possível aplicação em sistemas de fluxo contínuo.

Este estudo demonstrou que a fotocatálise heterogénea pode produzir peróxido de hidrogénio sob irradiação de luz visível utilizando derivados de biomassa (por exemplo, sacarídeos) como agentes de sacrifício, água do mar como solvente, e um catalisador isento de metal (nitreto de carbono grafítico). O mesmo cenário foi atingido ao utilizar o fotocatalisador imobilizado em dois suportes diferentes, o que constituiu a principal novidade deste trabalho, bem como a produção de peróxido de hidrogénio através da aplicação de biomassa e água do mar.

É crucial notar que esta tecnologia permite a geração no local deste combustível alternativo e, quando combinada com uma célula de combustível, pode potencialmente permitir a produção de eletricidade também no local. Como resultado, possui as principais características para ser considerada uma tecnologia promissora que pode ajudar a aliviar alguns dos desafios mais importantes do mundo.

# Declaration

I hereby declare, under word of honour, that this work is original and that all non-original contributions is indicated and due reference is given to the author and source

Porto, 4th of july 2022
Rita Amaral Borges

# Index

**1 Introduction ..... 1**

1.1 Framing and presentation of the work ..... 1

1.2 Contribution of the author to the work ..... 4

1.3 Main objectives ..... 5

1.4 Organization of the dissertation ..... 5

**2 Context and State of the art ..... 7**

2.1 Production of Hydrogen Peroxide ..... 7

2.2 GCN-T as a photocatalyst ..... 8

2.3 Principles of heterogeneous photocatalysis ..... 10

2.4 Searching for sustainable approaches ..... 11

**3 Materials and Methods ..... 15**

3.1 Reagents ..... 15

3.2 Catalyst preparation ..... 15

3.2.1 Synthesis of powder GCN-T ..... 15

3.2.2 Immobilization of the GCN-T photocatalyst ..... 16

3.3 Catalyst Characterization ..... 16

3.4 Photocatalytic experiments ..... 17

3.5 pH measurements ..... 18

3.6 Seawater preparation ..... 18

**4 Results and Discussion ..... 19**

4.1 Characterization of the powder photocatalysts ..... 19

4.1.1 FTIR-ATR analyses ..... 19

4.1.2 DR UV-vis measurements ..... 19

4.1.3 Solid State (PL) measurements ..... 20

4.1.4 Isotherms of the photocatalysts using BET method ..... 20

4.1.5 SEM analysis ..... 21

4.2 Characterization of the immobilized photocatalyst ..... 22

4.2.1 FTIR-ATR analyses ..... 22
4.2.2 DR UV-vis measurements ..... 23
4.2.3 Solid State PL measurements ..... 23
4.2.4 SEM analysis ..... 24
4.3 Photocatalytic $H_2O_2$ production ..... 25
4.3.1 Different saccharides as sacrificial agents ..... 27
4.3.2 Effect of the initial cellobiose concentration ..... 28
4.3.3 Effect of the presence of ions ..... 29
4.4 Photocatalytic $H_2O_2$ production using actual seawater ..... 31
4.5 GCN-T immobilized in a polymeric film ..... 32
4.5.1 Photocatalytic $H_2O_2$ production in UPW ..... 32
4.5.2 Reutilization experiments using the catalyst immobilized in a polymeric film .. 33
4.6 GCN-T immobilized in a 3D printed structure ..... 34
4.6.1 Photocatalytic $H_2O_2$ production in UPW ..... 34
4.6.2 Reutilization experiments using the 3D printed structure ..... 35
4.6.3 Photocatalytic $H_2O_2$ production in actual seawater using immobilized GCN-T ... 36
4.6.4 3D printed structure reuse using real seawater ..... 36
4.7 Apparent quantum efficiency ..... 37
**5 Conclusion ..... 39**
**6 Assessment of the work done ..... 41**
6.1 Objectives Achieved ..... 41
6.2 Final Assessment ..... 41
6.3 Limitations and recommendations for future work ..... 41
**7 References ..... 43**
**Appendix A. OceanOptics USB2000 + UV-vis spectrometer calibration curve ..... 47**
**Appendix B. Preparation of GCN-T ..... 48**
**Appendix C. Data for AQE calculations ..... 49**

# List of Figures

**Figure 1**. Average annual prices of oil per barrel through the years. ..... 2

**Figure 2.** Fresh water available in the world. ..... 4

**Figure 3.** Structure of g-$C_3N_4$, being tri-s-triazine ring structure circled in orange. ..... 8

**Figure 4.** Visualization of the main steps in heterogeneous photocatalysis (created in BioRender.com): i) light absorption, electron excitation and charge separation; ii) electron migration and ($e^-/h^+$) pairs recombination; iii) reduction/oxidation reactions; A, $A^-$) electron acceptor; D, D+) electron donor. ..... 10

**Figure 5.** Simplification of Figure 4, along with a potential reactional mechanism (created in BioRender.com). ..... 13

**Figure 6.** Setup of photocatalytic experiments (diagram created in BioRender.com), A corresponding to the catalyst in suspension, B immobilization of the catalyst on film, and C immobilization on a 3D structure: 1) Refrigeration system; 2) Glass reactor; 3) Air entrance; 4) LED (1 of 4 evenly distributed); 5) Fan to cool down the LED (1 of 4 equally distributed); 6) Magnetic bar; 7) Stirrer. ..... 17

**Figure 7.** FTIR results corresponding to DCN precursor, and bulk GCN and GCN-T materials. 19

**Figure 8.** DR UV-vis analyses of bulk GCN and GCN-T materials and LEDs energy flux. ..... 20

**Figure 9.** Photoluminescence spectra of bulk GCN and GCN-T powder photocatalysts. ..... 20

**Figure 10**. Adsorption and desorption isotherms: a) bulk GCN and b) GCN-T materials. ..... 21

**Figure 11.** Morphology of the powder photocatalysts: a) bulk GCN and b) GCN-T. ..... 21

**Figure 12.** a) FTIR-ATR results of uncoated and coated GCN-T film and powder GCN-T; b) FTIR-ATR spectra in the 1000 – 700 $cm^{-1}$ range. ..... 22

**Figure 13.** DR UV-vis analyses of the uncoated and coated GCN-T film and power GCN-T. ... 23

**Figure 14.** Photoluminescence spectra of GCN-T powder photocatalyst and uncoated and coated films. ..... 24

Figure 15. SEM images of a) uncoated film; b), c) and d) film coated with GCN-T; e) image of the GCN-T coated film. ..... 25

**Figure 16.** $H_2O_2$ concentration evolution using bulk GCN and GCN-T materials. Experimental conditions: 100 mL of an aqueous solution of 20 mM cellobiose (UPW); 1.0 g $L^{-1}$ catalyst load; and $\lambda_{max}$ = 412 nm. ..... 26

**Figure 17.** Effect of catalyst load in the production of $H_2O_2$. ..... 26

**Figure 18.** Effect of the use of different biomass derivatives. Experimental conditions: 100 mL of an 20 mM aqueous solution of sacrificial agent (UPW); 1.0 g $L^{-1}$ catalyst load (powder); and $\lambda_{max}$ = 412 nm..... 27

**Figure 19.** Effect of initial concentration of cellobiose. Experimental conditions: 100 mL of an aqueous solution of cellobiose (UPW); 1.0 g $L^{-1}$ catalyst load (powder); and $\lambda_{max}$ = 412 nm... 28

**Figure 20.** a) Comparison of the CLB and 2-propanol performance for producing $H_2O_2$. Experimental conditions: 100 mL of an 20 mM aqueous solution of sacrificial agent (UPW); 1.0 g $L^{-1}$ catalyst load (powder); and $\lambda_{max}$ = 412 nm; b) A 22-hour reaction with CLB as sacrificial agent. Experimental conditions: 100 mL of an 100 mM aqueous solution of sacrificial agent (UPW); 1.0 g $L^{-1}$ catalyst load (powder); and $\lambda_{max}$ = 412 nm. ..... 29

**Figure 21.** The effect of NaCl presence. Experimental conditions: 100 mL of an aqueous solution (UPW); 1.0 g $L^{-1}$ catalyst load (powder); and $\lambda_{max}$ = 412 nm..... 30

**Figure 22.** Effect of the remaining major constituent ions of seawater. Experimental conditions: 100 mL of an 100 mM aqueous solution (UPW) and 600 mM of NaCl; 1.0 g $L^{-1}$ catalyst load (powder); and $\lambda_{max}$ = 412 nm. ..... 31

**Figure 23.** The development of $H_2O_2$ concentration in UPW water, the generated synthetic mixture (SM), and actual seawater (SW) are compared. Experimental conditions: 100 mL of an aqueous solution; 1.0 g $L^{-1}$ catalyst load (powder); and $\lambda_{max}$ = 412 nm. ..... 32

**Figure 24.** $H_2O_2$ concentration evolution using GCN-T immobilized in a polymeric film. Experimental conditions: 100 mL of an aqueous solution of cellobiose (UPW); and $\lambda_{max}$ = 412 nm..... 33

**Figure 25.** $H_2O_2$ concentration after 3 hours of irradiation, using GCN-T immobilized in a polymeric film from 3 distinct reactions. Experimental conditions: 100 mL of an aqueous solution of 20 mM cellobiose (UPW); and $\lambda_{max}$ = 412 nm..... 34

**Figure 26.** Effect of initial concentration of cellobiose (20 mM and 100 mM) using powder and immobilized GCN-T. Experimental conditions: 100 mL of an aqueous solution of cellobiose (UPW); and $\lambda_{max}$ = 412 nm. ..... 35

**Figure 27.** a) $H_2O_2$ concentration after 3 hours of irradiation, using GCN-T immobilized in cylindrical structure design by additive manufacturing, from 3 different reactions. Experimental conditions: 100 mL of an aqueous solution of 20 mM cellobiose (UPW); and $\lambda_{max}$ = 412 nm; b) The GCN-T coated structure. ..... 35

**Figure 28.** Effect of initial concentration of cellobiose (20 mM and 100 mM). Experimental conditions: 100 mL of an aqueous solution of cellobiose using seawater (SW); and $\lambda_{max}$ = 412 nm. ..... 36

**Figure 29.** $H_2O_2$ concentration after 3 hours of irradiation, using GCN-T immobilized in cylindrical structure design by additive manufacturing, from 3 different reactions. Experimental conditions: 100 mL of an aqueous solution of 20 mM cellobiose using seawater (SW); and $\lambda_{max}$ = 412 nm. ..... 37

**Figure 30**. $H_2O_2$ concentration evolution using powder bulk, powder GCN-T, GCN-T coated film, and GCN-T coated structure. Experimental conditions: 100 mL of an aqueous solution of 20 mM cellobiose in UPW; and $\lambda_{max}$ = 412 nm. ..... 38

**Figure A1.** Calibration curve of OceanOptics USB2000 + UV–vis spectrometer for determination of $H_2O_2$ concentration. ..... 47

**Figure B1.** Steps to produce the catalyst: 1) dicyandiamide in semi-closed crucible; 2) semi-closed crucibles in the muffle furnace; 3) formation of bulk g-$C_3N_4$; 4) powdering of the bulk; 5) rinsing of the powdered bulk; 6) drying of the bulk on a drying oven; 7) powdered and rinsed bulk in an open crucible; 8) open crucible in the muffle furnace; 9) exfoliated GCN-T. ..... 48

**Figure B2.** Conditions of the thermal treatments applied to produce the catalyst..... 48

# List of Tables

**Table 1.** Different sacrificial agents employed. ..... 12

**Table 2.** Major ion composition of typical seawater [44]. ..... 14

**Table A1.** Values of the calibration curve of OceanOptics USB2000 + UV–vis spectrometer. .. 47

**Table C1.** Data related to the calculation of AQE of the different systems analyzed. ..... 49

# Notation and Glossary

### List of Symbols

| | | |
|---|---|---|
| $Ct$ | Concentration | mol $L^{-1}$ |
| $E_g$ | Energy band level | eV |
| $t$ | Time | s |
| $T$ | Temperature | ºC |
| $\lambda$ | Wavelength | nm |
| $n$ | Number of moles | mol |
| $P$ | intensity of irradiation light | J $s^{-1}$ $cm^{-2}$ |
| $S$ | Superficial area | $cm^2$ |
| $h$ | Plank constant | J s |
| $c$ | Speed of light | m $s^{-1}$ |
| $N_A$ | Avogadro constant | $mol^{-1}$ |
| $S_{BET}$ | Specific surface area | $m^2$ $g^{-1}$ |

### Indexes

| | |
|---|---|
| max | Maximum |

### List of Acronyms

| | |
|---|---|
| CB | Conduction band |
| VB | Valence band |
| $e^-$ | Electron |
| $h^+$ | Hole |
| g-$C_3N_4$ | Graphitic carbon nitride |
| DCN | Dicyandiamide |
| GCN | Bulk graphitic carbon nitride |
| GCN-T | Thermally exfoliated graphitic carbon nitride |
| $HO^\bullet$ | Hydroxyl radical |
| $H_2O_2$ | Hydrogen peroxide |
| $H_2$ | Hydrogen |
| LED | Light-Emitting Diode |
| $O_2$ | Oxygen |
| $O_2^{\bullet-}$ | Superoxide radical |
| ROS | Reactive Oxygen Species |
| DR UV-vis | Diffuse reflectance ultraviolet-visible |
| FTIR-ATR | Fourier transform infrared–attenuated total reflectance |
| PL | Photoluminescence |
| BET | Brunauer-Emmett-Teller |
| SEM | Scanning Electron Microscopy |
| HPLC | High Performance Liquid Chromatography |
| CLB | Cellobiose |
| UPW | Ultrapurified water |
| SW | Sea water |
| SM | Synthetic mixture |

# 1 Introduction

## 1.1 Framing and presentation of the work

Living in the world today allows us to contribute to the settlement of critical issues confronting humanity, while also envisioning a more prosperous, sustainable, and fair future in developing nations.

The 2030 Agenda for Sustainable Development was adopted in 2015 by all United Nations Member States and is based on 17 Sustainable Development Goals that demand maximal and urgent attention to enable a sustainable existence for humanity, the environment, and the planet itself before it is too late [1]. Poverty and hunger eradication, the prospect of good health and well-being, access to clean water and sanitation, clean and affordable energy, sustainable communities and cities, sustainable consumption and production, and climate action are some of the goals with great priority [1].

Indeed, climate change is one of the most worrying issues of our times. Gases (*e.g.*, carbon dioxide, methane, nitrous oxide, and other gases [2]) are generated and released into the atmosphere by different industrial sectors, thus being the main responsible for the worsening of the greenhouse effect, leading to harmful effects for both environment and humans. Related to the world greenhouse gas emissions in 2018, 48.9 Gt of carbon dioxide ($CO_2$) equivalent were emitted, a value that has been increasing annually [3]. The sector of energy is the one that most contributes to this expressive value, within which a large part is still powered by fossil fuels, as part of the generation of electricity, heat and to allow transportation [3].

In addition, the evolution of the world population has skyrocketed in recent decades. By 2100 it is expected that the world population reaches the $8.79 \times 10^9$ [4]. The peak of this evolution has not been reached, nevertheless, it is awaited to be accompanied by the demand for more electricity, fuels to allow the transportation of a higher number of persons and merchandise, and to power habitations, industries, and services. In particular, electricity consumption worldwide grows faster than any other energy source. In 1971, the annual world electric power consumption per capita was around 1.2 kW. In 2000, this value climbed to about 2.4 kW and in 2012, it reached a value close to 3.0 kW [5]. From 2012 to 2040 the global electricity generation may rise by 1.9 % $year^{-1}$ on average [6]. Therefore, it is expected that by 2050, the world will require two times more than its current energy supply [7].

Concerning fossil fuels, namely coal, oil, and gas, it is crucial to note that oil prices have been climbing, reflecting what is going on in the world. The highest average annual prices recorded were in 2013, around 108.56 US $ per barrel. In 2020, a barrel cost around 42 US $ as a result

of the COVID-19 pandemic. In 2021, it escalated to around 71 US $ per barrel and is forecast to have an average annual price of around 107.37 US $ per barrel in 2022, according to a June 2022 forecast, increasing dramatically after the invasion of Russia to Ukraine. The traders predict a meaningful shortage of supply due to sanctions placed on Russia [8].

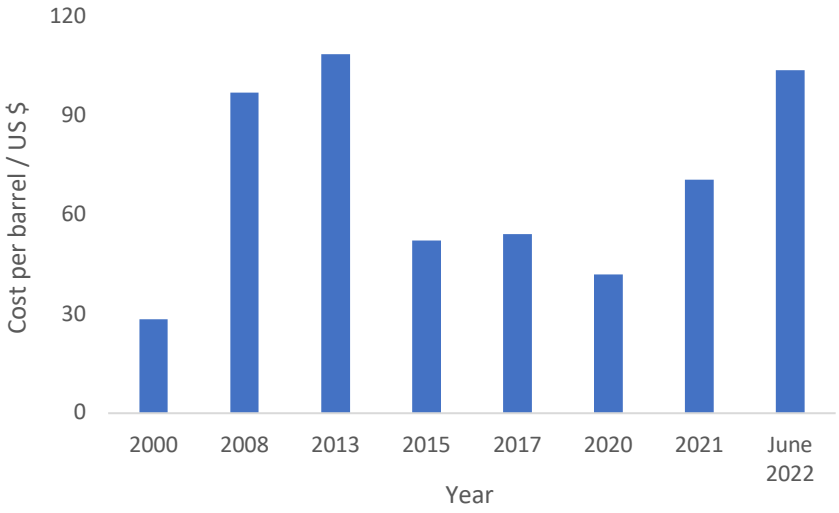



**Figure 1**. Average annual prices of oil per barrel through the years.

Most of the energy demand is derived from the usage of fossil fuels, such as oil, gas, and coal, but it is a finite resource that can run out. Oil is expected to be depleted by 2052, gas by 2060, and coal by 2090 [9].

Therefore, it is required to explore abundant renewable energy sources to replace fossil fuels. In addition, it should be noted that most global population growth would occur in less developed areas without grid access [4], thus technologies that produce energy that can be easily stored and/or allow on-site production of electricity and alternative fuels are necessary. Energy storage technologies are of most importance, not only for the integration of renewable sources in the grid, but also in several other aspects, such as energy backups, seasonal storage, quality, and safety in the input of electricity. As well as the contribution to achieving smart homes and smart grids [10], and in the transition from non-renewable energies to renewable in the use of hybrid electricity production systems.

Hydrogen peroxide ($H_2O_2$) is a versatile oxidant that produces only water as a byproduct and is commonly employed in organic synthesis and pulp bleaching [11]. Moreover, is used in some applications, *e.g.*, metal mining and processing, such as uranium extraction and purification, and in the production of stain-free detergents and holds disinfecting properties, which are quite required in pharmaceutical industries [12]. It is a high-demand product, with a global market share of ca. $4x10^9$ US $ predicted to expand to $5.2x10^9$ US $ in 2026 [13]. Its enormous energy

capacity, as well as its ease of storage and transportation, makes it more appealing than other typical green fuels, such as hydrogen ($H_2$). The energy density of aqueous $H_2O_2$ (70 wt %) is 3.1 MJ $L^{-1}$, which is quite comparable to $H_2$ (2.8 MJ $L^{-1}$) at 35 MPa (room temperature) when applied in fuel cells [14], bypassing the challenges associated with storing the latter. By being employed in a one-compartment fuel cell to generate electricity, it becomes a suitable energy carrier alternative to oil or hydrogen [15].

Developing a technology using sustainable components that securely generates on-site energy and/or conveniently stored alternative fuels without emitting greenhouse gases is of particular interest. In this view, artificial photosynthesis may be able to solve some of the concerns described above since this approach seeks to mimic nature's photosynthetic processes, allowing solar energy to be stored in high-energy chemical bonds [16]. If the reagents required are derived from infinite natural resources, high-value chemical compounds, and even alternative fuels, might be generated, this may constitute a great breakthrough for sustainability. Furthermore, the chemicals produced might be converted into electricity using fuel cells, permitting the safe production on-situ of both fuel and electricity while merging two complementary technologies [17].

Heterogeneous photocatalysis has been applied in different fields, including photocatalytic decomposition of pollutants [18], selective organic synthesis [19], disinfection, and energy storage [20]. Recently, semiconductor photocatalysis has been appointed as a promising technology for direct $H_2O_2$ generation aiming for the use of this chemical as a liquid and fossil-free fuel [15, 20]. The main advantages of this approach are the use of water as a solvent, the possibility of using biomass derivatives as sacrificial agents, and ideally the use of metal-free photocatalysts, which have already revealed high efficiency under light irradiation [21].

The use of water as a solvent to produce liquid fuels, such as $H_2O_2$, may be considered at a first sight an ideal solution. Although water covers 71 % of the Earth's surface, it is crucial to distinguish between different types of water based on their composition and source. Only 2.5 % of all world water is fresh water, 96.5 % is oceans, and the remainder is salty water. It has been recognized that the necessary water for the existence of humanity is already reduced, nevertheless, 68.7 % is preserved in glaciers and ice caps, 30.1 % is groundwater, and just 1.2 % is surface/other fresh water. The last one is 69 % constituted of ground ice and permafrost, with the remainder being the atmosphere, lakes, marshes, rivers, and living creatures [22].

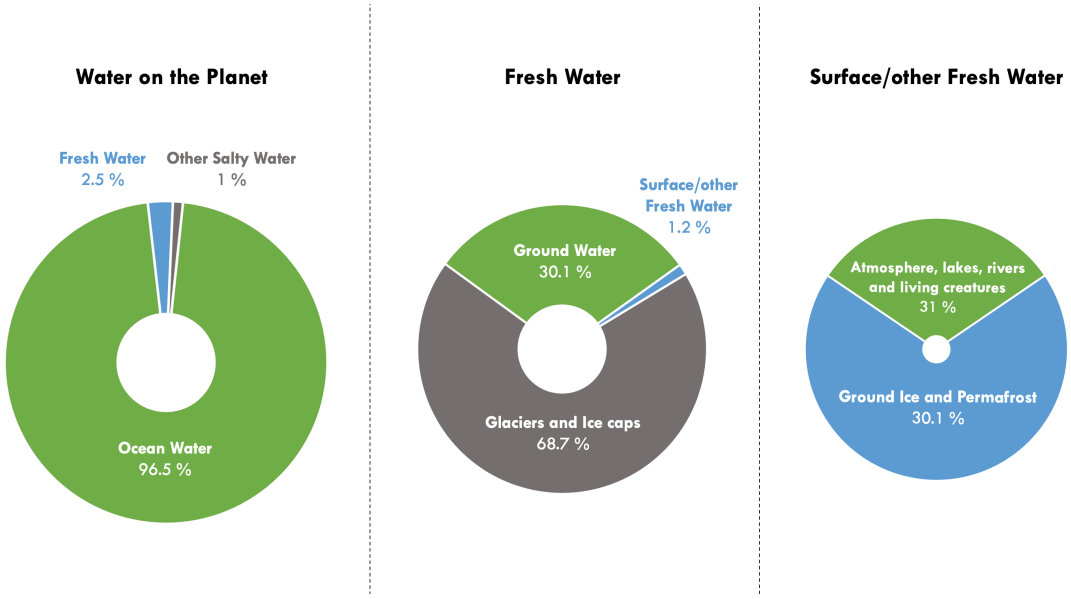



**Figure 2.** Freshwater available in the world.

The freshwater must be preserved to alleviate the problem of water resource scarcity, and thus, seawater (SW) could appear as a promising source due to its high availability and therefore process cost reduction [23].

Concerning the sacrificial agents that are commonly required in the production of $H_2O_2$ by photo-induced systems (*e.g.*, 2-propanol [24]), biomass derivatives constitute a sustainable alternative due to their abundancy [25].

Thus, this dissertation seeks the production of $H_2O_2$ using photo-induced systems, contributing to the advancement of photocatalysis technology in the energy field. The specific objectives are: i) preparation and characterization of optical semiconductors, namely graphitic carbon nitride (g-$C_3N_4$); ii) screening of different biomass derivatives as sacrificial agents (*e.g.*, sorbitol, arabinose, glucose, fructose, and cellobiose); iii) simulation of seawater using a synthetic solution and evaluate the effect of ionic species; iv) to develop different approaches for the photocatalyst immobilization and assess their efficiency for the production of $H_2O_2$; v) to assess $H_2O_2$ production with actual seawater using powder and immobilized thermally exfoliated graphitic carbon nitride (GCN-T) photocatalyst.

## 1.2 Contribution of the author to the work

During this study, I was involved in most of the experimental procedures including, the preparation and characterization of the powder photocatalysts and photocatalytic reactions for $H_2O_2$ production. In addition, I compiled the information on the state-of-art related to the $H_2O_2$ evolution using photo-induced systems and prepared the present dissertation report. The

photocatalytic setup (reactor and light-emitting diodes (LEDs)) was already available at the LSRE-LCM laboratory, and the immobilized photocatalysts were prepared by research team members involved in this work.

## 1.3 Main objectives

The major goal of the present work was to study the possibility of producing $H_2O_2$ by heterogeneous photocatalysis using a sustainable approach by using visible light for reaction activation and metal-free catalysts and to propose some insights regarding the mechanism of $H_2O_2$ production. For this, biomass was used as a sacrificial agent instead of products synthesized by polluting processes, and seawater was used to substitute potable water. Aiming at making the photocatalytic $H_2O_2$ production process more cost-effective, catalyst immobilization using different supports was investigated, allowing simple reuse of the catalyst, and avoiding the catalyst separation process.

## 1.4 Organization of the dissertation

There are six chapters in this dissertation. The current chapter provides a brief overview and describes the main purpose of the present study. In Chapter 2, the key concepts of heterogeneous photocatalysis are briefly explained, along with insights into the utilization of g-$C_3N_4$ for $H_2O_2$ generation and some information regarding it. The relevant innovative themes were also discussed. Chapter 3 contains a summary of the materials and methods. In Chapter 4, the characterization of various catalysts is presented, as well as the experimental reactions carried out with the aims indicated above and their corresponding interpretations. Chapters 5 and 6 are concerned with the findings and the assessment of the work done, respectively.

# 2 Context and State of the art

When we focus on solar energy, the major barrier of storage may be overcome in two ways. One of these involves the employment of two separate systems, solar cells paired with batteries, which may be linked by an external electrical circuit [17]. When there is no production, the electrical energy previously produced, which is stored in batteries, is then used. Alternatively, solar energy can be transformed into chemicals (liquid or gaseous) through photocatalytic processes. Then, these products can be physically stored, which can be converted into electricity anytime and anywhere using fuel cells.

A light-emitting source, water (proton donor), oxygen, a catalyst, and an electron donor all play important roles in the heterogeneous photocatalytic process. This combination allows the production of high-value chemicals such as hydrogen peroxide; however, to avoid deviating from the green path, the source of water, electron donor, and catalyst must be sustainable.

## 2.1 Production of Hydrogen Peroxide

By the year 2020, 95 % of $H_2O_2$ was produced through the hydrogenation of 2-alkyl-9,10-anthraquinone in dedicated chemical plants using organic solvents over a palladium catalyst [26]. The dihydroanthraquinone resulting from this reaction suffers fast oxidation in the presence of oxygen ($O_2$) to produce $H_2O_2$, with simultaneous regeneration of the anthraquinone [26]. This batch process requires the extraction of $H_2O_2$ from the solvent, catalyst separation and provides highly concentrated $H_2O_2$ solutions, which are unnecessary for most applications, posing as well safety risks in terms of storage and transport [26].

There is also a direct method of $H_2O_2$ production, avoiding the high energy cost that consists of the catalyzed direct contact of $H_2$ and $O_2$. Nevertheless, this reveals some problems, such as side reactions and decomposition of $H_2O_2$ in the presence of catalysts, the $H_2/O_2$ ratio in this process must be precisely controlled, as $H_2/O_2$ mixtures are explosive over a wide range of concentrations [17]. Thinners like as nitrogen, carbon dioxide, and argon can be added to the mixture to minimize the danger. Despite this, the method has not yet been dimensioned for industrial applications due to the remaining risk [26].

In this way, the production of $H_2O_2$ through artificial photosynthesis has appeared with many advantages. It can occur at normal pressure and temperature and the use of $H_2$ is not required, only water and oxygen are used as raw materials, both of which are quite abundant on the planet. The use of renewable sources can be used as an energy source, and the catalysts applied are optical semiconductors that pose no danger to the environment [26].

The water-splitting reaction in presence of oxygen driven by sunlight or a low-cost source of energy (*e.g.*, LEDs), has been identified as a promising prospective way for the green manufacturing of $H_2O_2$ [23].

## 2.2 GCN-T as a photocatalyst

An ideal semiconductor should be a substance that, when exposed to light, generates a chemical reaction that does not consume the material itself. In addition, an efficient photocatalyst must have the important features: i) chemically and biologically inert in nature; ii) capable of adsorbing reactants under photonic activation; iii) photo-stability; iv) availability and low cost; v) efficient charge separation by suppressing recombination; vi) insoluble in water; vii) nontoxic or low toxicity [27]. It should also restrict the decomposition of $H_2O_2$ once generated [27].

Several semiconductors have been studied and tested as photocatalysts for $H_2O_2$ production, which includes titanium dioxide ($TiO_2$) [28], metal-free resins [29], metal-organic frameworks [24], zinc oxide [30], and polymer-supported carbon dots [31].

Despite the efficiency of the reported photocatalysts, g-$C_3N_4$ is a material that shows high potential in this area. For $H_2O_2$ production, it is the most studied metal-free catalyst [21], with a band energy gap of about 2.7 eV which allows photo-activation in the visible range of the electromagnetic spectrum [18, 26]. Various precursors and modifications on its preparation have been explored, such as impregnation of gold nanoparticles [32], carbon doping [33], combination with carbon nanotubes [34], and creation of nitrogen vacancies [35]. This photocatalyst constituted entirely of Earth-abundant components (C, N, and H), a visible-light-responsive material with a graphitic stacking structure of melem sheets is regarded as a fully sustainable catalyst [7].

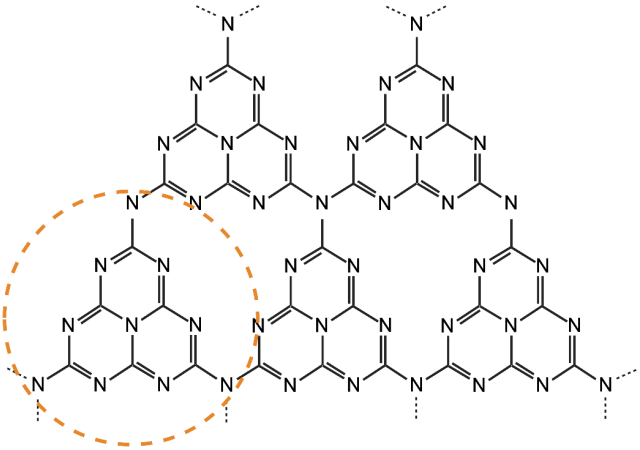


**Figure 3.** Structure of g-$C_3N_4$, being tri-s-triazine ring structure circled in orange.

According to published research, g-$C_3N_4$ holds a significant photocatalytic efficiency for water splitting when exposed to visible light [36], which is quite important if the main goal is the production of $H_2O_2$, since excitation using UV-light (< 400 nm) decomposes $H_2O_2$ into hydroxyl radicals, while the $e^-$ in the conduction band (CB) reduces $H_2O_2$ due to their low-lying reduction potentials [37]. Being g-$C_3N_4$ a metal-free catalyst and absorbing in the visible zone above 400 nm [38], the breakdown of the $H_2O_2$ produced can be prevented. In addition, the temperature of the system should be carefully examined because the $H_2O_2$ also degrades as the temperature rises owing mostly to the LEDs' intensity. By controlling these factors (irradiation and temperature), photocatalysis technology becomes a very promising alternative for $H_2O_2$ production.

The high electron/hole recombination rate caused by Van der Walls interactions between g-$C_3N_4$ layers, low quantum efficiency, and tiny specific area are some of the disadvantages of using g-$C_3N_4$ materials in photocatalysis. As described above, methods such as metal doping, combination with carbon materials, thermal treatments, and others have been used to increase the specific surface area of these photocatalysts [18]. The bulk g-$C_3N_4$ (here labeled as GCN), used in the present study exhibit these undesirable features. Nevertheless, several previous works proved that when bulk g-$C_3N_4$ is subjected to a thermal exfoliation procedure, the resulting material (here labeled as GCN-T) holds several desirable physicochemical properties, such as higher specific surface area [18, 19].

Following light excitation, electron/hole recombination, and electron migration, the latter reacts with adsorbed molecular oxygen and hydroxyls to produce reactive oxygen species (ROS). The oxygen reduction reaction (ORR) by photogenerated electrons route, one electron or two electrons, plays a critical role in the overall reaction on the semiconductor conduction band since it not only inhibits electron-hole recombination but also generates ROS. $H_2O_2$ is produced on the photocatalyst bulk's surface via an $O_2$ single-electron reduction route, whereas two-electron reduction happens on the surface of the photocatalyst nano sheets [7]. In the latter, the fast synthesis of 1,4-endoperoxide removes two electrons from the photocatalyst practically instantaneously, stabilizing two holes and making them available for reaction. Contrary, because the reduction reaction requires only one electron on the bulk's surface, there will be fewer stable holes available, resulting in a decrease of $H_2O_2$ production. One probable reason consists of the surface's energy of g-$C_3N_4$ rising following exfoliation, therefore the g-$C_3N_4$ photocatalysts may choose to recombine with $O_2$ to stabilize their states, enabling the synthesis of 1,4-endoperoxide [39].

Concerning the technological approach for $H_2O_2$, in general, the use of photocatalysts in powder form is highly efficient compared with immobilized catalysts. Nevertheless, the immobilization is favorable because it facilitates the separation of the catalyst from the reaction mixture, the

isolation of reaction products, the recovery and recycling of the catalyst, as well may allow the application of continuous flow procedures [40].

## 2.3 Principles of heterogeneous photocatalysis

In a classical heterogeneous photocatalytic reaction, the overall process includes 3 main steps (Figure 4):

i) Photons are absorbed in a semiconductor photocatalyst, and if the energy of the photon is greater than the photocatalyst's band gap ($E_g$), electrons in the valence band (VB) are excited to the CB, creating holes in the VB and allowing the formation of positively charged holes;

ii) The photoinduced electrons ($e^-$) and holes ($h^+$) split, and the electrons travel to the photocatalyst's surface, while some $e^-/h^+$ pairs can recombine at the catalyst surface;

iii) The charge carriers react with the chemical species on the photocatalyst's surface [26].

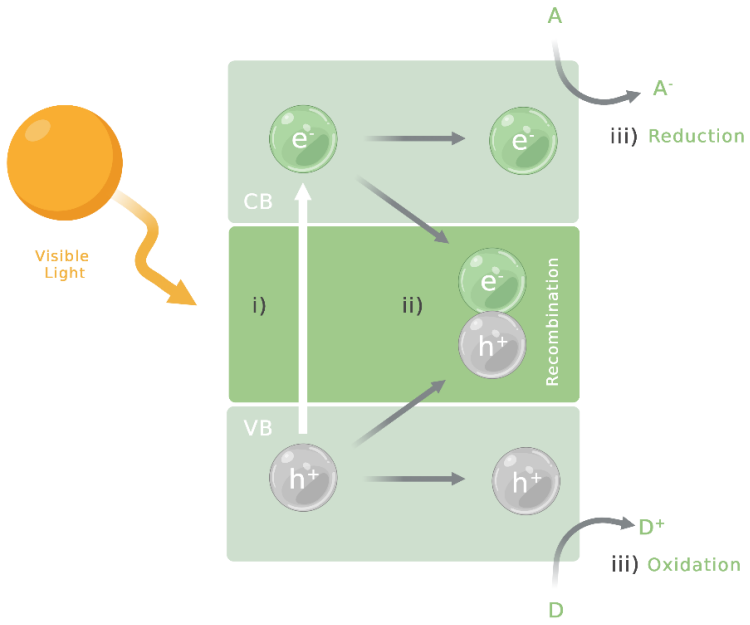



**Figure 4.** Schematic representation of the main steps in heterogeneous photocatalysis (created in BioRender.com): i) light absorption, electron excitation and charge separation; ii) electron migration and ($e^-/h^+$) pairs recombination; iii) reduction/oxidation reactions; A, $A^-$) electron acceptor; D, D+) electron donor.

The photocatalyst should benefit two-electron oxygen reduction over a four-electron reaction (equations 1 to 5). Even though the last one is more thermodynamically favorable, is more advantageous for chemical-to-electrical conversion technologies, such as fuel cells [12].

It has been previously mentioned that g-$C_3N_4$ materials, activated by visible light using water-containing alcohols (*e.g.*, ethanol, propan-2-ol, and butan-2-ol) as sacrificial agents in presence

of $O_2$ preferentially enhance two-electron reduction of $O_2$ while inhibiting subsequent photodecomposition of the generated $H_2O_2$.

$$O_2 + (H^+ + e^-) \rightarrow HOO^* \quad \textbf{(1)}$$

$$HOO^* + (H^+ + e^-) \rightarrow H_2O + O^* \quad \textbf{(2)}$$

$$O^* + (H^+ + e^-) \rightarrow HO^* \quad \textbf{(3)}$$

$$HO^* + (H^+ + e^-) \rightarrow H_2O \quad \textbf{(4)}$$

$$O_2 + 4(H^+ + e^-) \rightarrow 2\,H_2O \quad E^0 = 1.23\ V_{RHE} \quad \textbf{(5)}$$

The effective production of 1,4-endoperoxide species on the surface of the photoexcited g-$C_3N_4$ results in a selective two-electron reduction of $O_2$ [11], benefiting the $H_2O_2$ production.

In this way, a photovoltaic system capable of producing $H_2O_2$ will consist of 3 parts. First, upon light excitation, the electron donor plays its part by enabling electrons to occupy certain holes, freeing the corresponding electron to react. Some holes in the VB would then oxidize $H_2O$, producing $O_2$ and protons (equation 6). The electrons in the CB would then react with the adsorbed $O_2$ to produce $H_2O_2$. Equations 7 to 10 represent the indirect sequential two-step single-electron reduction pathway, equation 11 the direct one-step two-electron reduction, and equation 12 the overall photocatalytic reaction [26].

$$2\,H_2O + 4\,h^+ \rightarrow O_2 + 4\,H^+ \quad \textbf{(6)}$$

$$O_2 + e^- \rightarrow O_2^{\bullet -} \quad \textbf{(7)}$$

$$O_2^{\bullet -} + H^+ \rightarrow HO_2^{\bullet -} \quad \textbf{(8)}$$

$$HO_2^{\bullet -} + e^- \rightarrow HO_2^- \quad \textbf{(9)}$$

$$HO_2^- + H^+ \rightarrow H_2O_2 \quad \textbf{(10)}$$

$$O_2 + 2\,H^+ + 2\,e^- \rightarrow H_2O_2 \quad \textbf{(11)}$$

$$2\,H_2O + O_2 \xrightarrow{h\nu} H_2O_2 \qquad \Delta G^0 = 117\ kJ\ mol^{-1} \quad \textbf{(12)}$$

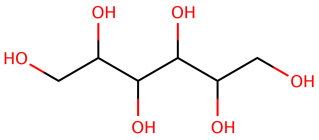
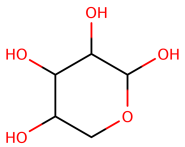
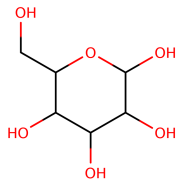
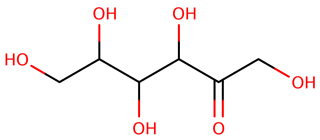
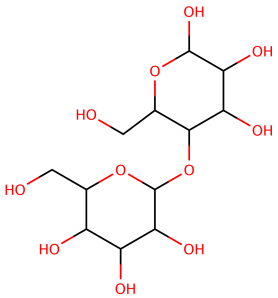
## 2.4 Searching for sustainable approaches

It is essential to explore different sacrificial agents that are abundant, ecologically friendly and do not release harmful substances. Because biomass is a renewable energy source, it is an excellent choice for the conversion into value-added chemical molecules. It can replace the consumption of raw materials generated by a polluting process as sacrificial agents, increasing the process sustainability.

Carbohydrates, particularly mono-, di-, and polysaccharides that serve as sacrificial electron donors, have already attracted interest in $H_2$ synthesis via photocatalysis. This breakthrough

has already been explored with noble metal-loaded $TiO_2$ catalysts [41] and CNT-$TiO_2$ composites [42]. Despite this, as far as my knowledge, the utilization of g-$C_3N_4$ based materials for $H_2O_2$ photocatalytic through biomass-derived chemicals was not yet discussed in the literature. The compounds selected in this work were sorbitol, arabinose, glucose, fructose, and cellobiose (Table 1).

**Table 1.** Different sacrificial agents employed.

| Compound | Chemical structure | Important properties |
|---|---|---|
| Sorbitol<br>$C_6H_{14}O_6$ |  | **Molecular Weight:** 182.17 / g mol$^{-1}$<br>**Solubility:** 220 g 100 mL$^{-1}$ (20 °C) |
| Arabinose<br>$C_5H_{10}O_5$ |  | **Molecular Weight:** 150.13 / g mol$^{-1}$<br>**Solubility:** 83.4 g 100 mL$^{-1}$ (25 °C) |
| Glucose<br>$C_6H_{12}O_6$ |  | **Molecular Weight:** 180.16 / g mol$^{-1}$<br>**Solubility:** 91 g 100 mL$^{-1}$ (25 °C) |
| Fructose<br>$C_6H_{12}O_6$ |  | **Molecular Weight:** 180.16 / g mol$^{-1}$<br>**Solubility:** 440 g 100 mL$^{-1}$ (25 °C) |
| Cellobiose<br>$C_{12}H_{22}O_{11}$ |  | **Molecular Weight:** 342.29 / g mol$^{-1}$<br>**Solubility:** 12 g 100 mL$^{-1}$ (25 °C) |

Because of their H:C molar ratio, they are particularly appealing, and it could be explored how their intrinsic characteristics and structural complexity may have an impact on $H_2O_2$ photocatalytic generation.

When water is oxidized by $h^+$ (equation 6), the saccharides, acting as sacrificial agents, are expected to be oxidized. Because saccharides have comparable properties to alcohols relating to -OH groups, it is possible that the reaction process is nearly identical. It's proposed that based on already studied and published reaction mechanisms for oxidation of alcohols [11, 43], the chemical route in this work, could be as following (being equation 15 the general reaction):

$$R_2 - CHOH + h^+ \rightarrow R_2 - CHO^- + H^+ \quad \textbf{(13)}$$

$$R_2 - CHO^- + h^+ \rightarrow R_2 - CO^{\bullet -} + H^+ \quad \textbf{(14)}$$

$$R_2 - CHOH + 2\,h^+ \rightarrow R_2 - CO^{\bullet -} + 2\,H^+ \quad \textbf{(15)}$$

As a result, the reaction mechanism for photocatalytic $H_2O_2$ production using saccharides as a sacrificial agent may be as shown in Figure 5:

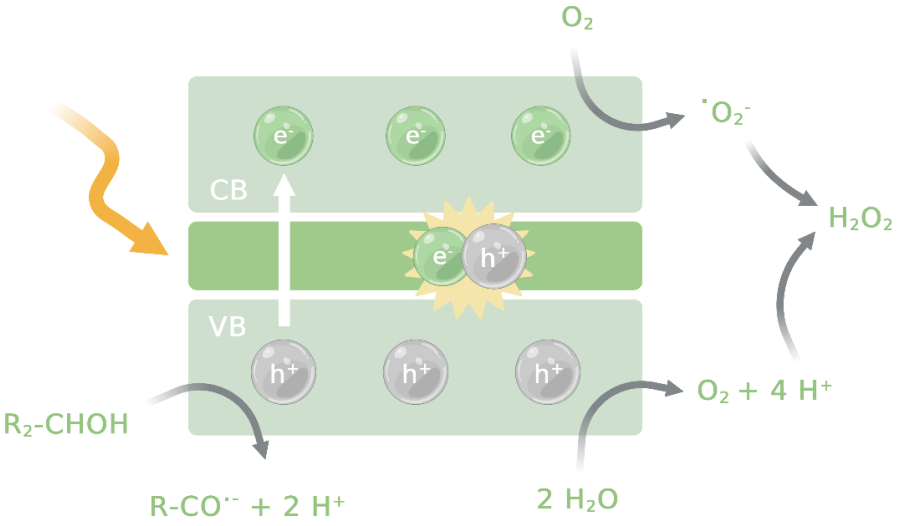



**Figure 5.** Simplification of Figure 4, along with a potential reactional mechanism (created in BioRender.com).

The salinity of seawater ranges from 33 to 38 ppt of NaCl, with an average of 35 ppt [44], and constituted of various dissolved ions depending on the region, the most important of which are listed in Table 2. Despite the presence of additional components that are naturally present in seawater such as, sand and algae, as well contaminants resulting from human activities, their influence were not explored in the present study. As a limitless natural water resource, seawater appears as great opportunity to investigate the effective $H_2O_2$ production.

**Table 2.** Major ion composition of typical seawater [45].

| Constituent | Concentration / mg $L^{-1}$ |
|---|---|
| Chloride ($Cl^-$) | 18980 |
| Sodium ($Na^+$) | 10556 |
| Sulfate ($So_4^{-2}$) | 2649 |
| Magnesium ($Mg^{2+}$) | 1262 |
| Calcium ($Ca^{2+}$) | 400 |
| Potassium ($K^+$) | 380 |

Therefore, this study brings some benefits in the field of $H_2O_2$ production by photo-induced systems, such as the use of seawater, which is a limitless natural resource, thus is avoided the consumption of the world's potable water. The use of biomass derivatives can be an alternative for synthetic chemical substances described in literature. The process can be photoactivated by solar light by utilizing a catalyst that absorbs in the visible range, while being composed of non-toxic components (metal-free). Moreover, the immobilization of the catalyst could simplify the overall process by eliminating the catalyst separation and allow a continuous flow reaction system. As a result, combining a green technology for the synthesis of a value-added product with natural raw materials, a totally sustainable $H_2O_2$ production method may be achievable.

# 3 Materials and Methods

## 3.1 Reagents

Hydrogen peroxide ($H_2O_2$, 27 wt. % in water, Sigma-Aldrich), sulfuric acid ($H_2SO_4$, 95 %, Fluka), titanium (IV) oxysulphate ($TiO_5S$, ~15 wt. % in sulphuric acid, Sigma-Aldrich) and ultrapurified water (UPW) were used to prepare a set of standard samples of known concentration aiming the determination of the calibration curve of $H_2O_2$ through colorimetric method.

Dicyandiamide ($C_2H_4N_4$, 99 %, Sigma-Aldrich) was used as precursor for the synthesis of GCN, and then was used to produce GCN-T.

D-Sorbitol ($C_6H_{14}O_6$, 99 %, Alfa Aesar), D(-)-Arabinose ($C_5H_{10}O_5$, 99+ %, Acros Organics), D(-)-Fructose ($C_6H_{12}O_6$, 99 %, Acros Organics), D-(+)-Glucose, anhydrous ($C_6H_{12}O_6$, 98 %, Alfa Aesar) and D(+)–Cellobiose ($C_{12}H_{22}O_{11}$, 98 %, Acros Organics) were tested individually as sacrificial agents.

Sodium chloride (NaCl, >99.9 %, José Manuel Gomes dos Santos, LDA) was used to simulate salty water, and calcium chloride ($CaCl_2$, >99.9 %, Fisher Scientific UK), magnesium chloride ($MgCl_2$, 98 %, Sigma), potassium chloride (KCl, >99.9 %, José Manuel Gomes dos Santos, LDA) and sodium sulfate ($Na_2SO_4$, >99.9 %, Sigma-Aldrich) were combined with the salty water to synthesize seawater.

## 3.2 Catalyst preparation

### 3.2.1 Synthesis of powder GCN-T

The synthesis of bulk GCN was performed by thermal decomposition of the dicyandiamide by following a similar procedure described elsewhere [19]. The precursor was placed in a closed crucible in a microwave muffle furnace Phoenix™ (CEM Corporative) under a static air atmosphere. The equipment was programmed to heat at a 2 ºC $min^{-1}$ ramp until 450 ºC, over a period of 1 hour and half, maintaining after this value for 50 minutes. Subsequently, it was heated until 550 ºC for 1 hour, then the temperature was maintained for 30 minutes, finishing the first thermal treatment. Afterward, the material was powdered in a mortar, rinsed with ultrapurified water, filtered, and dried overnight in a drying oven [18]. Then, a second thermal treatment was performed on the bulk GCN, producing an exfoliated material designated as GCN-T. This catalyst was synthesized by placing 0.95 g of bulk GCN in an open crucible inside a microwave furnace programmed to heat at 2 °C $min^{-1}$ until 500 °C, then this temperature was maintained for 2 h under a static air atmosphere [18].

### 3.2.2 Immobilization of the GCN-T photocatalyst

For the immobilization of the GCN-T two different approaches were applied, as follows:

At room temperature, a solution containing 0.070 g of polyvinylpyrrolidone (PVP) and 6.0 mL of 1-methyl-2-pyrrolidone (NMP) was sonicated for 3 hours. After that, 1.07 g of polyvinylidene fluoride (PVDF) was added, and the polymerization process began at 40 °C for 48 hours. The polymer solution was then kept unstirred at room temperature overnight to allow air bubbles to escape.

To prepare the flat film (55.68 $cm^2$) the polymer solution was applied with a knife casting applicator (Elcometer 3580, Warren, MI), and a certain amount of GCN-T powder was spread on top of the polymeric film before followed by its immersion in distilled water.

Moreover, a cylindrical structure to immobilize the GCN-T was designed and produced in a 3D printer BEETHEFIRST using Polylactic Acid plastic filament. For the immobilization of GCN-T in the cylindrical structure (149.66 $cm^2$), a thin film of the polymer solution was spread with a brush and a certain amount of GCN-T powder was spread on the structure.

## 3.3 Catalyst Characterization

The catalysts were characterized using a variety of techniques.

Fourier transform infrared–attenuated total reflectance (FTIR-ATR) measurements (4000–600 $cm^{-1}$) were recorded on a JASCO FT/IR-6800 spectrometer (JASCO Analytical Instruments, USA) equipped with a MIRacleTM Single Reflection ATR (attenuated total reflectance ZnSe crystal plate) accessory (PIKE Technologies, USA). The analysis was performed using 256 scans with a resolution of 4 $cm^{-1}$.

The diffuse-reflectance ultraviolet–visible (DR UV–vis) analyses were carried out in a JASCO V-560 UV–vis spectrophotometer equipped with an integrating sphere attachment (JASCO ISV-469).

Solid-state photoluminescence (PL) spectra were obtained at room temperature in a fluorescence spectrofluorometer (JASCO, FP-8300) equipped with a 150 W Xenon lamp, using both excitation and emission bandwidths fixed at 2.5 nm. The emission spectra were recorded upon excitation at 370 nm in the 390−700 nm range.

The Brunauer-Emmett-Teller (BET) specific surface area ($S_{BET}$) was determined through the $N_2$ adsorption data at −196 °C in the relative pressure range 0.05 – 0.20, using a Quantachrome NOVA 4200e apparatus.

The morphology of the photocatalysts GCN and GCN-T were examined by scanning electron microscopy (SEM) using a FEI Quanta 400 FEG ESEM/EDAX Genesis X4M (15 keV) microscope. The

morphology of the selected immobilized GCN-T photocatalyst was examined by scanning electron microscopy (SEM) using a Phenom ProX apparatus.

## 3.4 Photocatalytic experiments

Photocatalytic studies were carried out in a glass reactor under light irradiation using a visible four LED system with an emission line peaking at 412 nm placed symmetrically at 3.0 cm from the reactor wall. The average irradiance of the LEDs system reaching the reactor wall was 139 mW $cm^{-2}$ distributed evenly by the four sides of the box that surrounded the reactor. The photocatalytic setup is displayed in Figure 6.

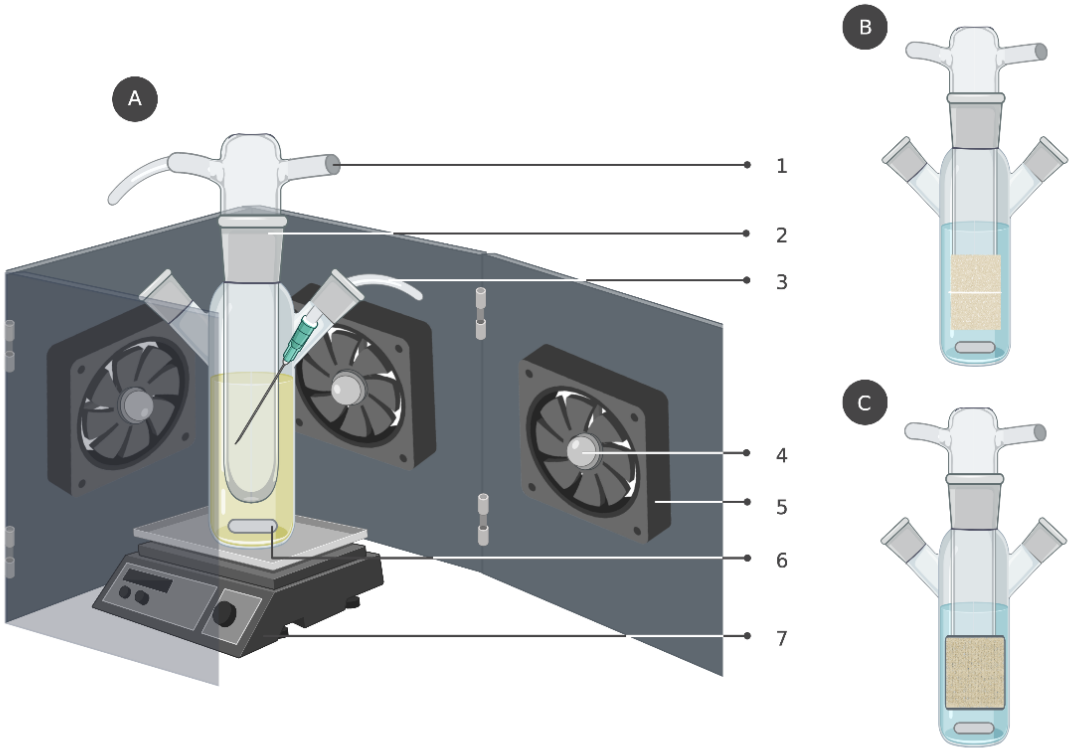



**Figure 6.** Setup of photocatalytic experiments (diagram created in BioRender.com), A corresponding to the catalyst in suspension, B immobilization of the catalyst on film, and C immobilization on a 3D structure: 1) Refrigeration system; 2) Glass reactor; 3) Air entrance; 4) LED (1 of 4 evenly distributed); 5) Fan to cool down the LED (1 of 4 equally distributed); 6) Magnetic bar; 7) Stirrer.

In a typical experiment, 100 mL of an aqueous solution containing a selected sacrificial agent (*e.g.*, sorbitol, arabinose, fructose, glucose, and cellobiose) were introduced into the reactor. Then, 1 g $L^{-1}$ of the powder photocatalyst was added and sonicated in an ultrasonic bath for 10 seconds. Similar reaction conditions were used in case of the catalyst immobilized on the two supports. The final suspension (or solution in case of the reaction using immobilized catalyst) was stirred and left for in dark conditions for 30 minutes before turning on the LEDs to achieve the adsorption/desorption equilibrium. During the photocatalytic process, the aqueous

solutions were continuously bubbled with air, magnetically agitated, and cooled with a refrigeration system.

The samples were withdrawn from the reactor, filtered using Teknokroma syringe filters PTFE 0.2 μm 13 mm ∅ (when used the catalyst in powder form), and the concentration of $H_2O_2$ was followed by the colorimetric technique using an UV-vis spectrophotometer.

The concentration of $H_2O_2$ produced during photocatalytic reactions was determined using the colorimetric method [46]. In a polystyrene cuvette, 300 μL of the filtered sample, 300 μL of 0.5 M $H_2SO_4$, and 10 μL of titanium (IV) oxysulphate were combined, and the absorbance was measured at 405 nm using an OceanOptics USB2000 + UV–vis spectrometer.

To avoid contamination, the material was collected separately for each polystyrene cuvette using a different pipette tip. To facilitate mixing and reaction, after the addition of $H_2SO_4$ to the sample, the tip was dipped in it to release titanium (IV) oxysulphate. This is only conceivable because a different tip was also used for each cuvette.

## 3.5 pH measurements

The pH of the reaction media was measured before and after the reaction using the WTW inoLab pH/ION 7320.

## 3.6 Seawater preparation

In this study, the seawater used was collected in the district of *Porto* in Northern Portugal, more specifically in *Póvoa de Varzim*.

The only treatment given to seawater was a vacuum filtration, which was accomplished with a CEM vacuum bomb using VWR EuropeanCat glass microfibers filters 693 47 MM.

# 4 Results and Discussion

## 4.1 Characterization of the powder photocatalysts

The characterization of the powder photocatalysts was examined using distinct techniques described as follows:

### 4.1.1 FTIR-ATR analyses

The FTIR-ATR studies were performed to validate the transition of DCN (dicyandiamide) precursor into graphitic carbon nitride materials, especially the formation of the characteristic tri-s-triazine ring structure. A peak ascribed to 805 $cm^{-1}$ appears in both GCN and GCN-T materials, indicating its formation (Figure 7) [47]. The peak indicative of a triple covalent bond between a carbon and a nitrogen atom, which is part of the DCN structure, emerges around 2200 $cm^{-1}$ only for DCN precursor and does not appear for the carbon nitride materials, suggesting that the thermal decomposition of DCN into carbon nitride materials was accomplished.

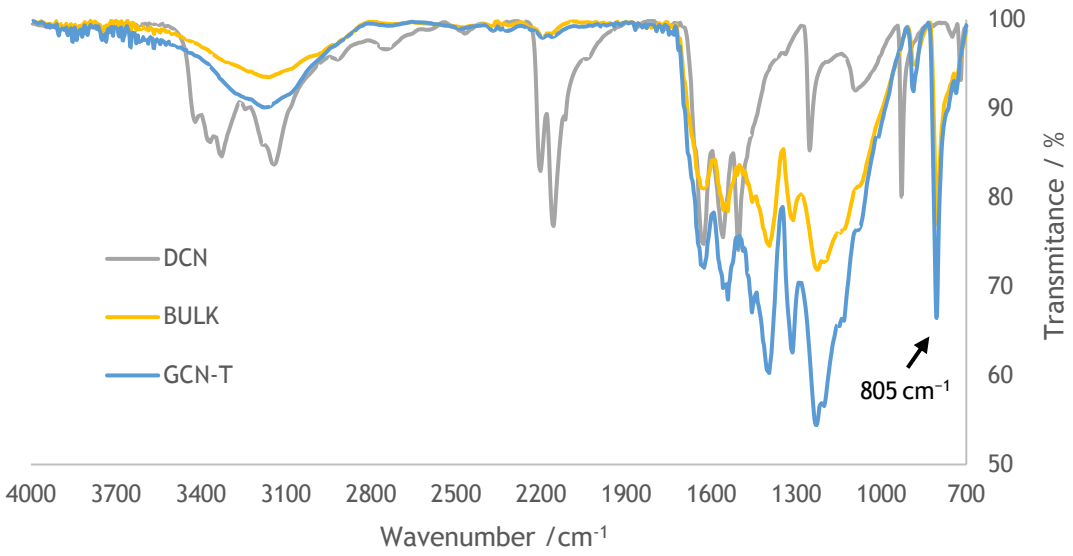



**Figure 7.** FTIR results corresponding to DCN precursor, bulk GCN, and GCN-T materials.

### 4.1.2 DR UV-vis measurements

The DR UV-Vis spectra of GCN and GCN-T materials show an unresolved broad band fading out between 450 and 500 nm, being maximum absorbance observed around 378 nm and 372 nm for bulk GCN and GCN-T materials, respectively (Figure 8). This is indicative that these materials absorb light in the visible range, which is particularly important if the main goal is the application of visible light sources, such as the one used in the present study ($\lambda_{max}$ = 412 nm).

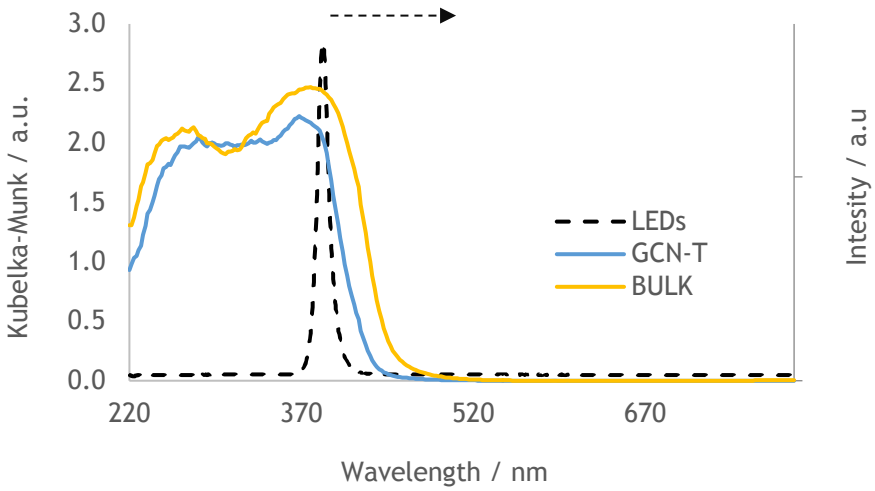



**Figure 8.** DR UV-vis analyses of bulk GCN and GCN-T materials and LEDs energy flux.

### 4.1.3 Solid State (PL) measurements

As displayed in Figure 9, maximum intensity is observed around 466 nm and 463 nm for bulk GCN and GCN-T materials, respectively. This higher intensity value has been described as a stronger luminescence in the excited state. This is reflected in a higher number of excited states that are accessible to the reaction, suggesting that the GCN-T is more efficient in the photocatalytic process compared to bulk GCN.

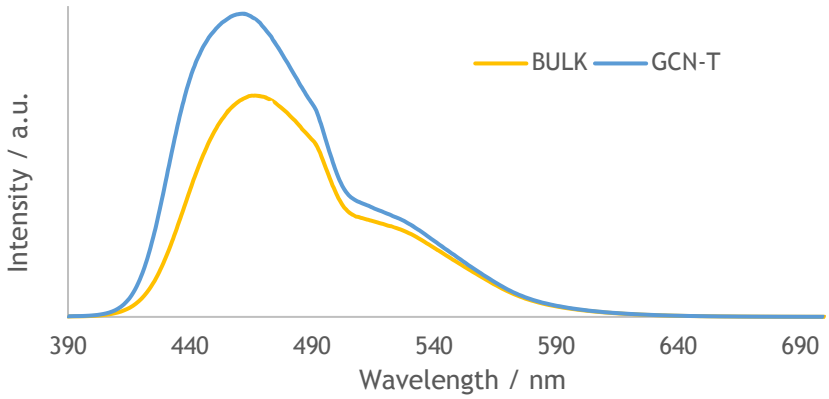



**Figure 9.** Photoluminescence spectra of bulk GCN and GCN-T powder photocatalysts.

### 4.1.4 Isotherms of the photocatalysts using BET method

As displayed in Figure 10 both materials show a type II adsorption isotherm and type H3 hysteresis, which suggests the presence of wedge-shaped pores [48].

The $S_{BET}$ of the bulk g-$C_3N_4$ materials prepared by direct pyrolysis of dicyandiamide is described in the literature as typically quite low [19]. This was also observed, with the bulk GCN revealing a small $S_{BET}$ (7 $m^2$ $g^{-1}$). Nevertheless, after thermal post-treatment at 500 °C, the $S_{BET}$ of the resulting material (GCN-T) increased to 105 $m^2$ $g^{-1}$ ca. 15 times higher.

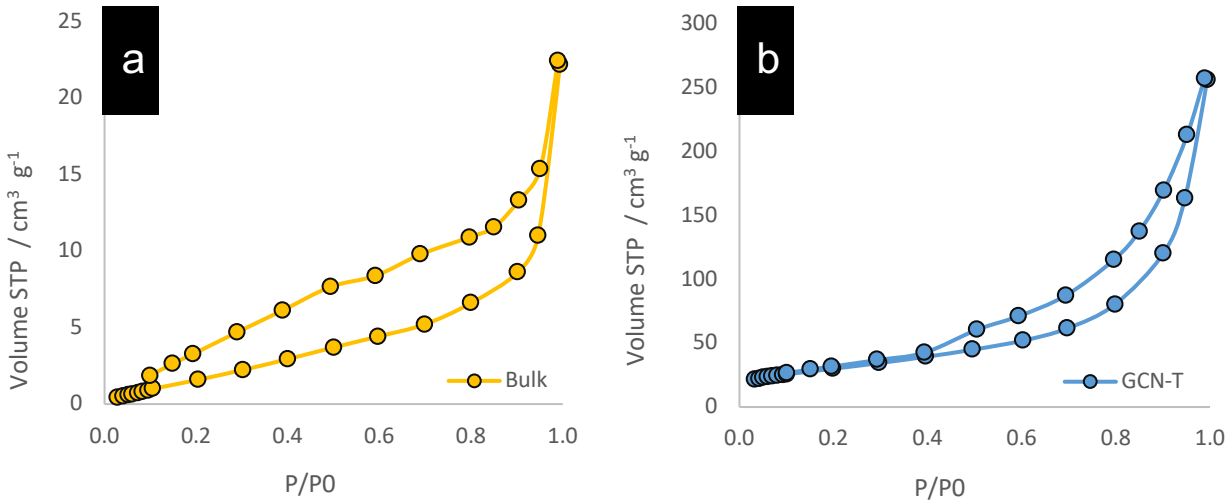



**Figure 10.** Adsorption and desorption isotherms: a) bulk GCN and b) GCN-T materials.

### 4.1.5 SEM analysis

As observed by SEM images (Figure 10), the bulk GCN seems to be constituted by dense aggregates. The GCN-T appears to be made up of overlapping sheets that have been laminated, which is consistent with the increased surface area. Considering all this information, both catalysts exhibit photo stimulation and the characteristics required to allow $H_2O_2$ production to a certain extent. However, it is found that GCN-T is the best catalyst for this process because it has more excited states accessible to react when photo stimulated and a larger surface area.

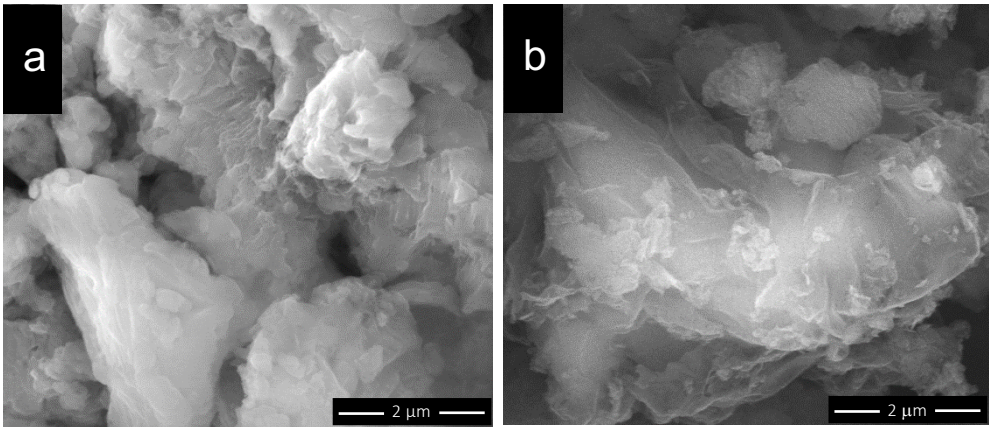



**Figure 11.** Morphology of the powder photocatalysts: a) bulk GCN and b) GCN-T.

## 4.2 Characterization of the immobilized photocatalyst

### 4.2.1 FTIR-ATR analyses

The chemical structure of the immobilized catalyst was analyzed by FTIR-ATR and for comparison purposes, the uncoated film and the GCN-T powder were also exhibited (Figure 7). It is observed similar spectra for both uncoated and coated GCN-T film, suggesting that the selected scan zone is covered by the polymer and the GCN-T is hidden. The broad band observed for uncoated and coated GCN-T films from 3100 and 3700 $cm^{-1}$ can be ascribed to O-H bonds to adsorbed water on the polymer surface. In addition, from FTIR-ATR spectra is observed similar profiles for both uncoated and coated GCN-T film, suggesting that the analyzed zone is covered by the polymer and the GCN-T is eventually hidden. However, there is a minor peak at 805 $cm^{-1}$ that is not detected in the uncoated film (Figure 12b). This peak is ascribed to characteristic tri-s-triazine ring structure, although it is negligibly shifted to the left, suggests the presence of the GCN-T catalyst deposited on the polymer surface, implying that it could be photo stimulated.

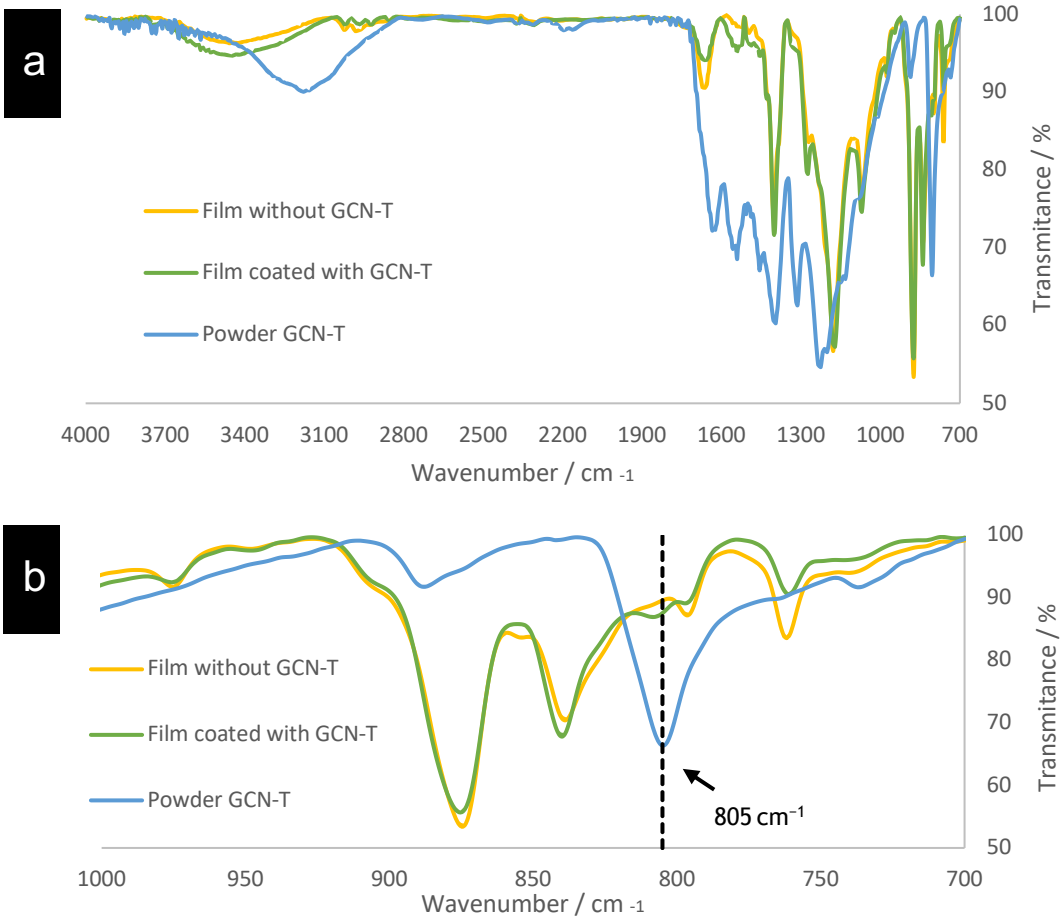



**Figure 12.** a) FTIR-ATR results of uncoated and coated GCN-T film and powder GCN-T; b) FTIR-ATR spectra in the 1000 – 700 $cm^{-1}$ range.

### 4.2.2 DR UV-vis measurements

As observe in Figure 13 the film coated with GCN-T also absorb at the LEDs emission wavelength (412 nm). At this wavelength, the absorbance of GCN-T powder and GCN-T coated film is nearly identical. However, when the entire spectrum is examined, the absorbance of the film coated with GCN-T is remarkably comparable to the one of powder GCN-T, albeit slightly lower in value and possibly smoothed out. This might be due to the immersion phase in distilled water that accompanies the impregnation of the GCN-T in the film. When the polymer is emerged in water, it may suffuse portions of the catalyst, generating a tiny translucent layer above.

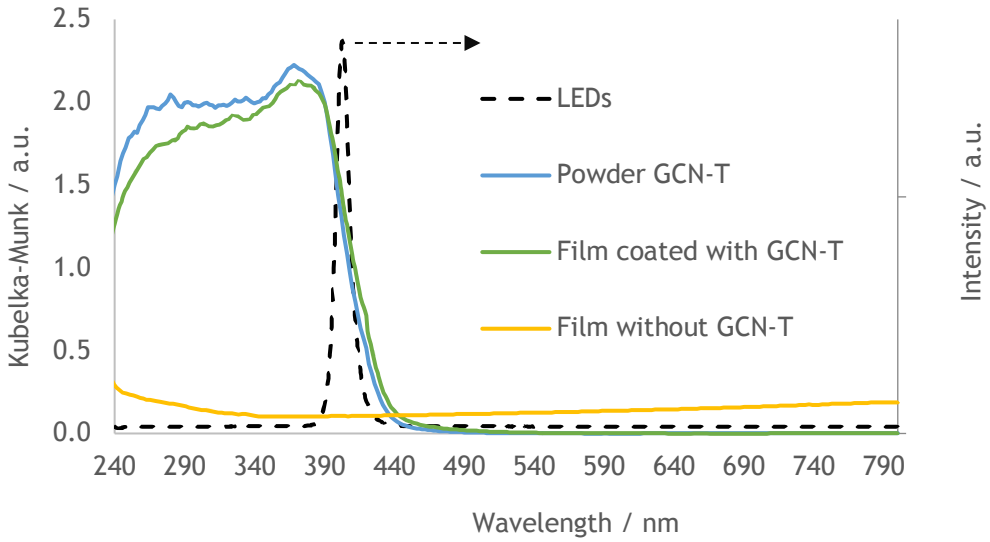



**Figure 13.** DR UV-vis analyses of the uncoated and coated GCN-T film and power GCN-T.

### 4.2.3 Solid State PL measurements

To investigate the occurrence of electron-hole charge separation and transfer upon light excitation PL analyses were performed. As observed the powder GCN-T presents a higher intensity value, suggesting that a greater number of excited states that are available for the reaction. The film coated with GCN-T has a substantially lower intensity value, indicating that there are fewer reaction sites accessible. Because the uncoated film shows negligible intensity, the coated GCN-T film meets the intensity response of both in the middle. This might be justified by the formation of the previously mentioned polymer layer, which covers a portion of the catalyst, allowing it to have a reduced intensity when photo stimulated.

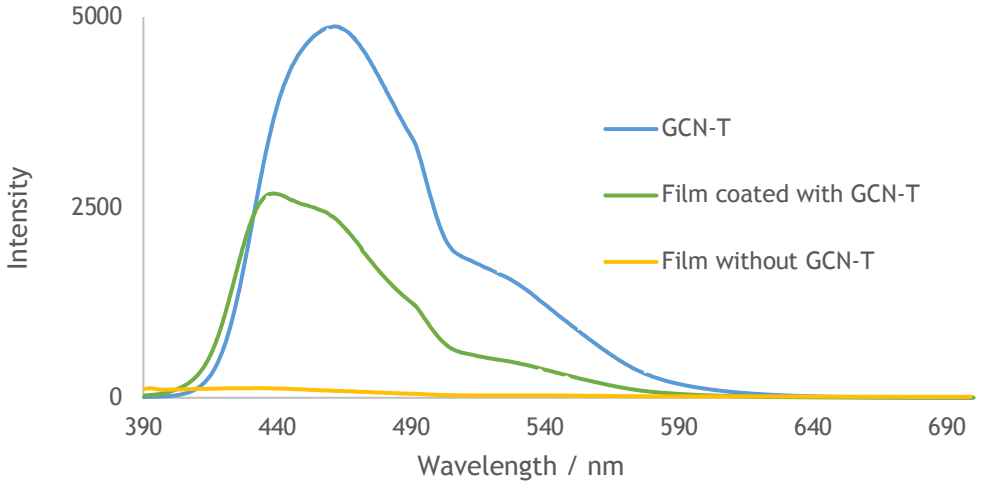



**Figure 14.** Photoluminescence spectra of GCN-T powder photocatalyst and uncoated and coated films.

### 4.2.4 SEM analysis

The morphology of the uncoated and coated GCN-T film was examined by SEM. Figure 15a, shows the SEM image of uncoated film, which exhibits a smooth appearance. Nevertheless, when powder GCN-T material has attached it is clearly visible the presence of the catalyst (Figure 15b). In Figure 15c), the portion to be analyzed was cut with scissors and as shown is detected the presence of powdered GCN-T catalyst. The cut is not straight, resulting in a concavity that enables a greater view of the inside of the region (Figure 15d). However, it was a cut that went all the way through the film, and it appears that portion of the catalyst piece is at the level of the polymer, not simply above and on the surface of it. This image appears to imply that, as previously stated, when the polymer is immersed in distilled water, a little layer of polymer may cover a portion of the catalyst.

In Figure 15e, it is shown an image of the film coated with GCN-T placed around the refrigeration system inside the reactor. Even though the catalyst dispersion was uniform during the GCN-T deposition, some material clusters were developed, which can be seen by naked eye. This may explain the FTIR-ATR analysis, which seems that the presence of GCN-T is almost negligible. Probably, it will be important to perform a full scan of the coated GCN-T film to find possible characteristic bands of the photocatalyst.

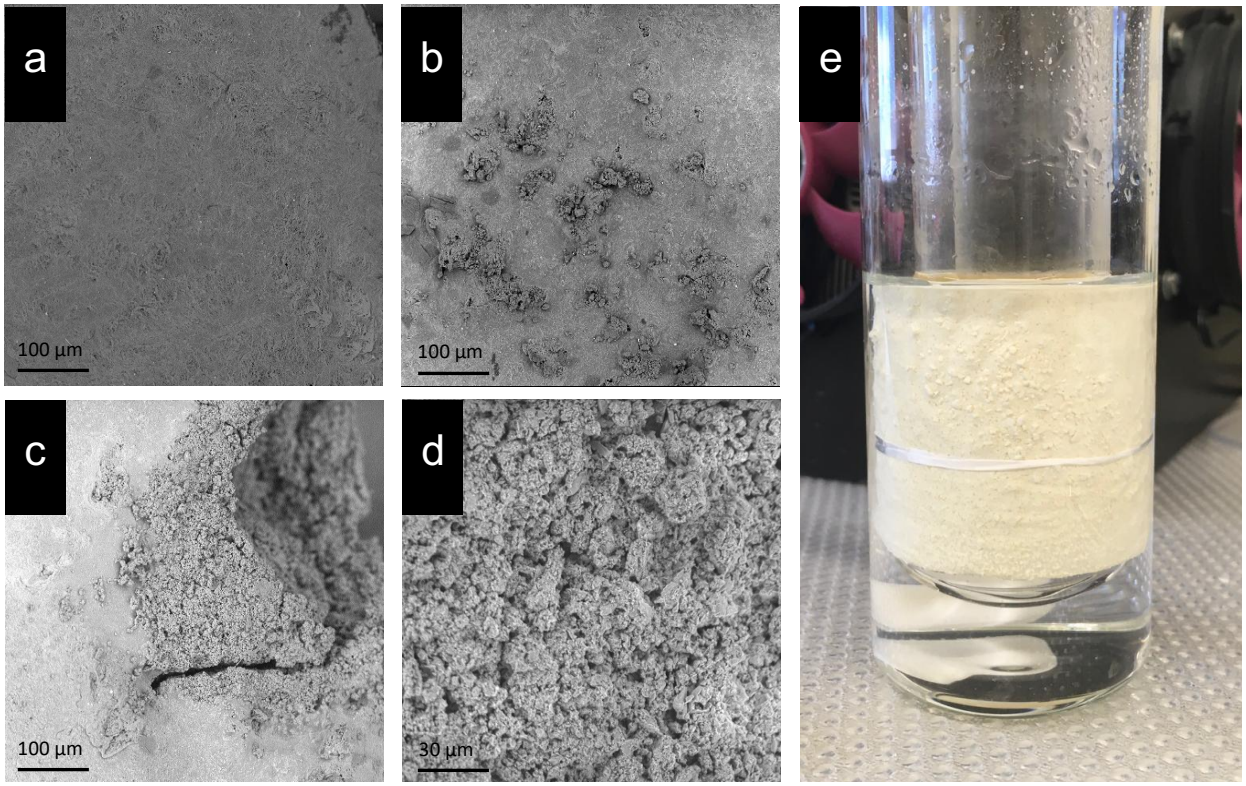



**Figure 15.** SEM images of a) uncoated film; b), c) and d) film coated with GCN-T; e) image of the GCN-T coated film.

## 4.3 Photocatalytic $H_2O_2$ production

During the photocatalytic experiments, various parameters were evaluated, including the screening of several sacrificial agents, initial concentration of a selected sacrificial agent, the pH of the solutions, catalyst load, the use of a synthetic and actual seawater solution, and the immobilization of the catalyst in two ways.

Nevertheless, since the bulk GCN and the GCN-T were prepared materials, it was performed a primary test to prove the better efficiency of the GCN-T photocatalyst as already been described in the literature for several photo-induced applications [18, 21]. A calibration curve of $H_2O_2$ was performed before the experiment to follow the $H_2O_2$ production during the photocatalytic reactions (Figure A1, supplementary data). As shown in Figure 16, the bulk GCN revealed a lower efficiency for $H_2O_2$ production compared with the exfoliated GCN-T material, which can be ascribed to the small specific surface area of the bulk GCN (7 $m^2$ $g^{-1}$) in comparison with the GCN-T (105 $m^2$ $g^{-1}$).

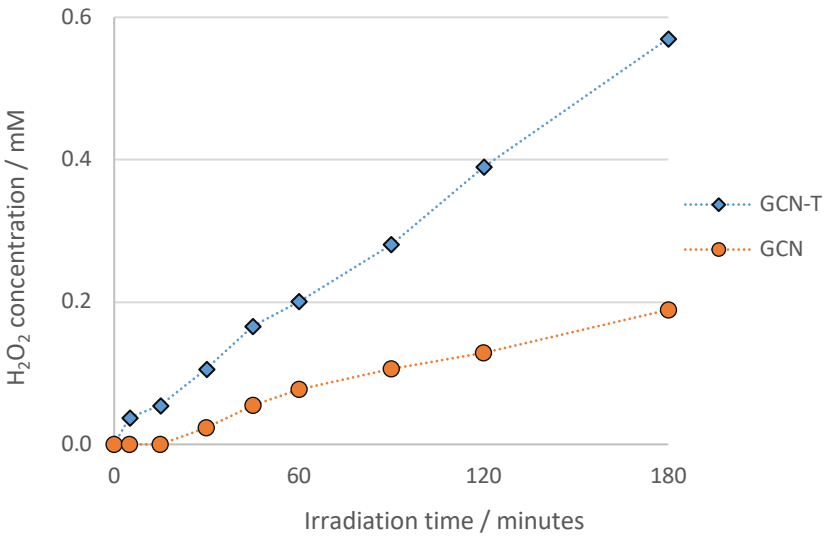



**Figure 16.** $H_2O_2$ concentration evolution using bulk GCN and GCN-T materials. Experimental conditions: 100 mL of an aqueous solution of 20 mM of CLB (UPW); 1.0 g $L^{-1}$ catalyst load; and $\lambda_{max}$ = 412 nm.

To understand if the reaction is ruled by heterogenous photocatalysis the catalyst load was evaluated between 0 and 1.75 g $L^{-1}$ (Figure 17). In these experiments, it was used 100 mM aqueous solution of cellobiose as sacrificial agent under visible light irradiation ($\lambda_{max}$ = 412 nm). In absence of catalyst no production of $H_2O_2$ was observed. In addition, by increasing the catalyst load until 1.5 g $L^{-1}$ an enhancement in the $H_2O_2$ production was observed, confirming the heterogeneous regime. Taking into consideration the negligible difference (~6 %) between $H_2O_2$ production using 1.0 and 1.5 g $L^{-1}$ of catalyst load, the study was followed using 1.0 g $L^{-1}$ of photocatalyst.

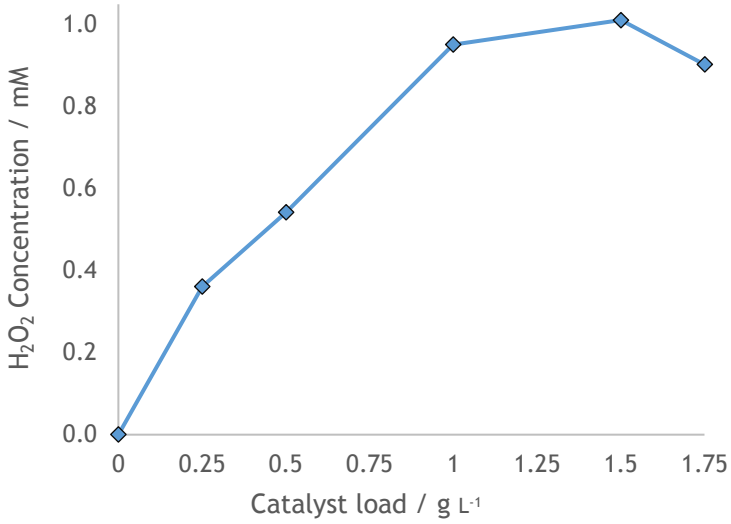



**Figure 17.** Effect of catalyst load in the production of $H_2O_2$.

### 4.3.1 Different saccharides as sacrificial agents

As mentioned before the presence of sacrificial agent for $H_2O_2$ production during the photocatalytic process is of great importance, thus various biomass derivatives were used as sacrificial agents due to the presence of -OH groups in their chemical structure (Figure 18).

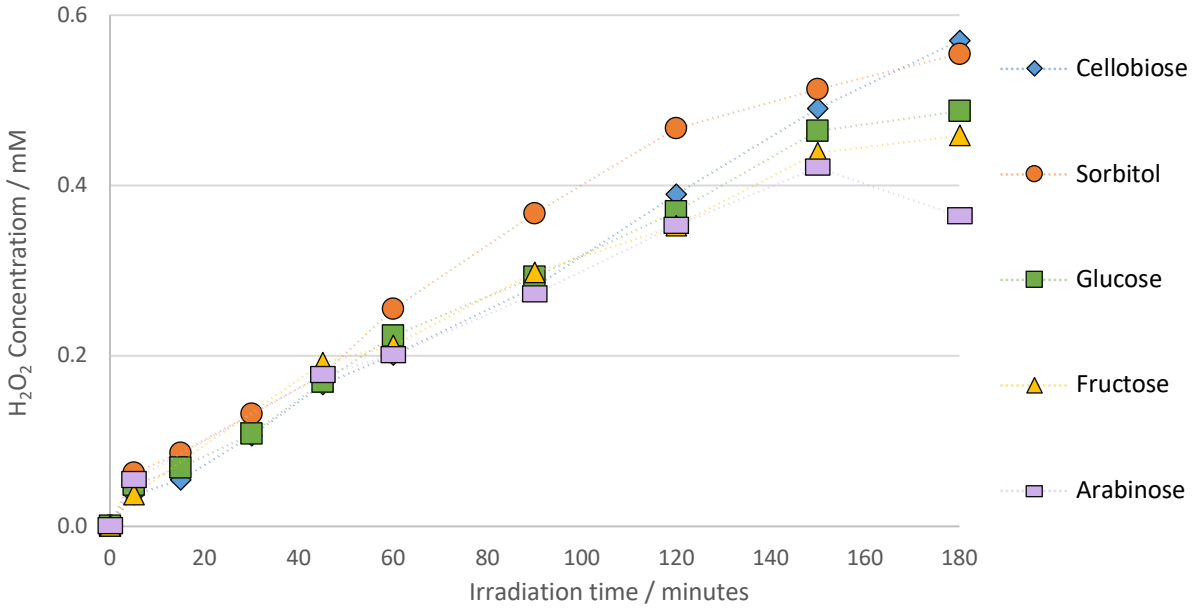



**Figure 18.** Effect of the use of different biomass derivatives. Experimental conditions: 100 mL of an 20 mM aqueous solution of sacrificial agent (UPW); 1.0 g $L^{-1}$ catalyst load (powder); and $\lambda_{max}$ = 412 nm.

In general, it appears that there is a relation between the amount of $H_2O_2$ generated and the number of -OH groups in the molecule, in ascending order as follows: arabinose < fructose = glucose < sorbitol < cellobiose (Figure 18). When compared, the saccharides with the lowest yield were arabinose and fructose, even though there was low variation between all of them. After 3 hours, with arabinose it was produced 0.364 mM of $H_2O_2$ and with fructose it was obtained 0.458 mM. Although sorbitol reveled greater values for most time values, it appears to achieve a plateau around 180 minutes of reaction, whereas cellobiose seems to follow a growing trend. After 3 hours of irradiation, was obtained with sorbitol 0.554 mM of $H_2O_2$ and with cellobiose was achieved 0.570 mM.

Because glucose and fructose have a similar chemical formula and differ only in structural complexity, the latter parameter may be analyzed separately when comparing the evolution of $H_2O_2$ generation with these two saccharides. Despite that nearly the same quantity of $H_2O_2$ was produced, it can be considered that at least the complexity of the structure does not significantly affect $H_2O_2$ formation. Per this line of thought, despite its structural complexity, cellobiose might be a candidate for the saccharide that allows the highest $H_2O_2$ generation due to its high number of -OH groups.

### 4.3.2 Effect of the initial cellobiose concentration

The cellobiose revealed the highest efficiency for $H_2O_2$ production, thus the initial concentration of this biomass derivative was evaluated aiming the increase of $H_2O_2$ concentration. As displayed in Figure 19, increasing the initial concentration of cellobiose 100 times the concentration of $H_2O_2$ was raised from 0 mM to 1.848 mM, for initial concentrations of 1.0 mM and 100 mM, respectively. In addition, is important to refer that in absence of sacrificial agent (0 mM) no formation of $H_2O_2$ was detected.

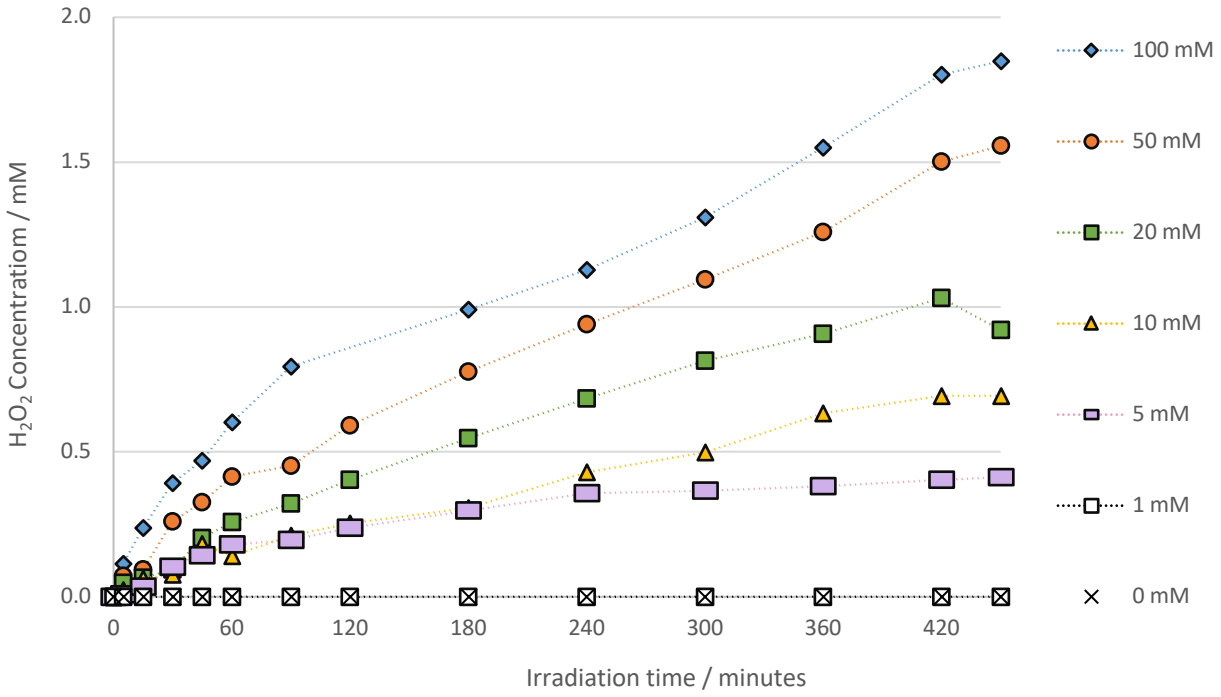



**Figure 19.** Effect of initial concentration of cellobiose. Experimental conditions: 100 mL of an aqueous solution of cellobiose (UPW); 1.0 g $L^{-1}$ catalyst load (powder); and $\lambda_{max}$ = 412 nm.

Because alcohols are commonly used as sacrificial agents in photocatalytic production of $H_2$ and $H_2O_2$, the performance of cellobiose was compared to that of 2-propanol, which is a model molecule used for this purpose [24]. Cellobiose performs about the same as 2-propanol for the first 3 hours (Figure 20a), demonstrating the potential of biomass, specifically saccharides, as a sacrificial agent.

To access the stability of the $H_2O_2$ produced, a 22-hour reaction was made divided by 3 days since a laboratory system with these features should not be left on for extended periods of time unsupervised. Also, to collect enough samples to track the evolution from one day to the next, the LEDs, air intake, and magnetic stirring were all switched off. To avoid a temperature rise in the solution, the cooling system was kept running at a lower flow rate than the operating one. One sample was taken when the reaction was stopped, and another when it was restarted.

While the absorbance of these two samples was compared, it was found that the value differed insignificantly, demonstrating that $H_2O_2$ does not degrade when the temperature of the solution is kept constant and in the dark. This demonstrated that the GCN-T catalyst is active for at least 22 hours, producing 4.590 mM of $H_2O_2$. In addition, it was observed that the system seems to follow a growing trend, which may indicate that the biomass concentration used is probably in excess.

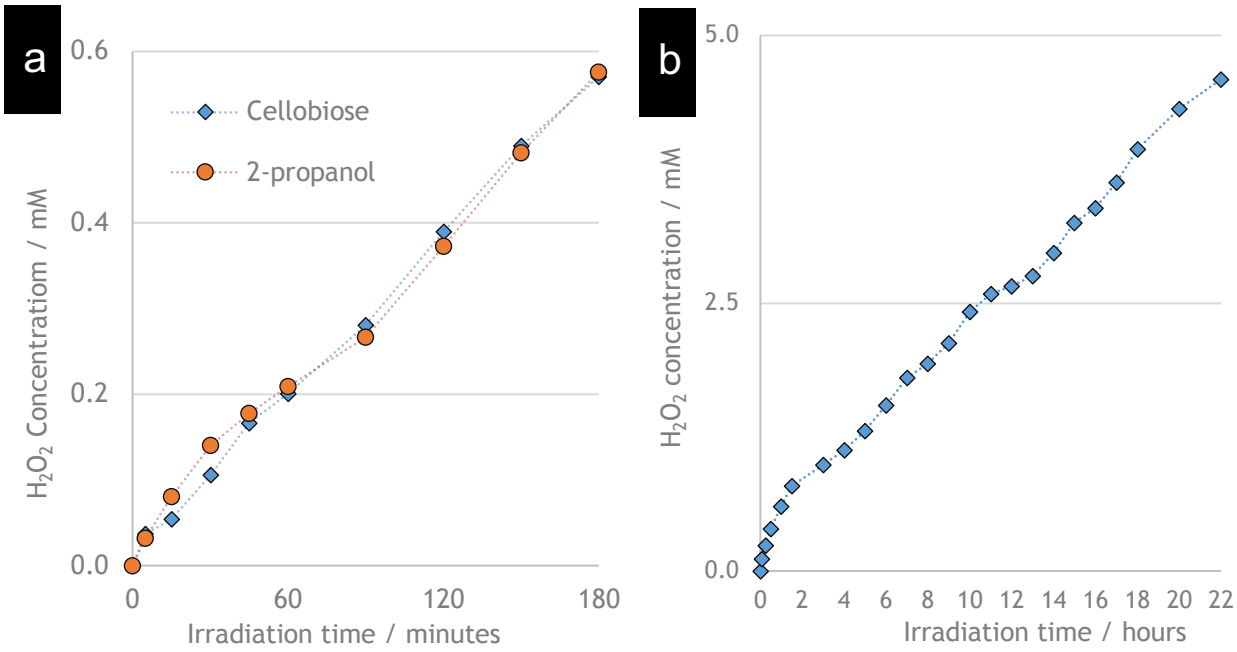



**Figure 20.** a) Comparison of the cellobiose and 2-propanol performance for producing $H_2O_2$. Experimental conditions: 100 mL of an 20 mM aqueous solution of sacrificial agent (UPW); 1.0 g $L^{-1}$ catalyst load (powder); and $\lambda_{max}$ = 412 nm; b) A 22-hour reaction with cellobiose as sacrificial agent. Experimental conditions: 100 mL of an 100 mM aqueous solution of sacrificial agent (UPW); 1.0 g $L^{-1}$ catalyst load (powder); and $\lambda_{max}$ = 412 nm.

### 4.3.3 Effect of the presence of ions

Before adding the ions commonly present in seawater, it was performed a preliminary experiment using NaCl to analyze its isolated impact on $H_2O_2$ production [49]. To an UPW solution with CLB was added NaCl to mimic the average salinity of 600 mM of seawater. This corresponds to a saline concentration of 35 %. The presence of salt, as shown in Figure 21, allows a greater formation of $H_2O_2$. After 6 hours, it was generated 4.587 mM of $H_2O_2$. When the $H_2O_2$ evolution from two equal initial solutions differing only in the addition of the salt is compared, it was found that with this addition it was produced, after 6 hours, practically the same amount of $H_2O_2$ produced as in a 22-hour reaction without the salt (Figure 20b). This implies a significant benefit over what it commonly means to operate with seawater: perhaps

desalination will not be required. As a result, seems that it there is no need to put this water to an exceedingly energy consuming using expensive treatments [50].

Following up, a reaction with only UPW and 600 mM of NaCl was performed, and no $H_2O_2$ was produced. This shows that NaCl does not act as a sacrificial agent, and only enhances the photocatalytic process in the presence of cellobiose.

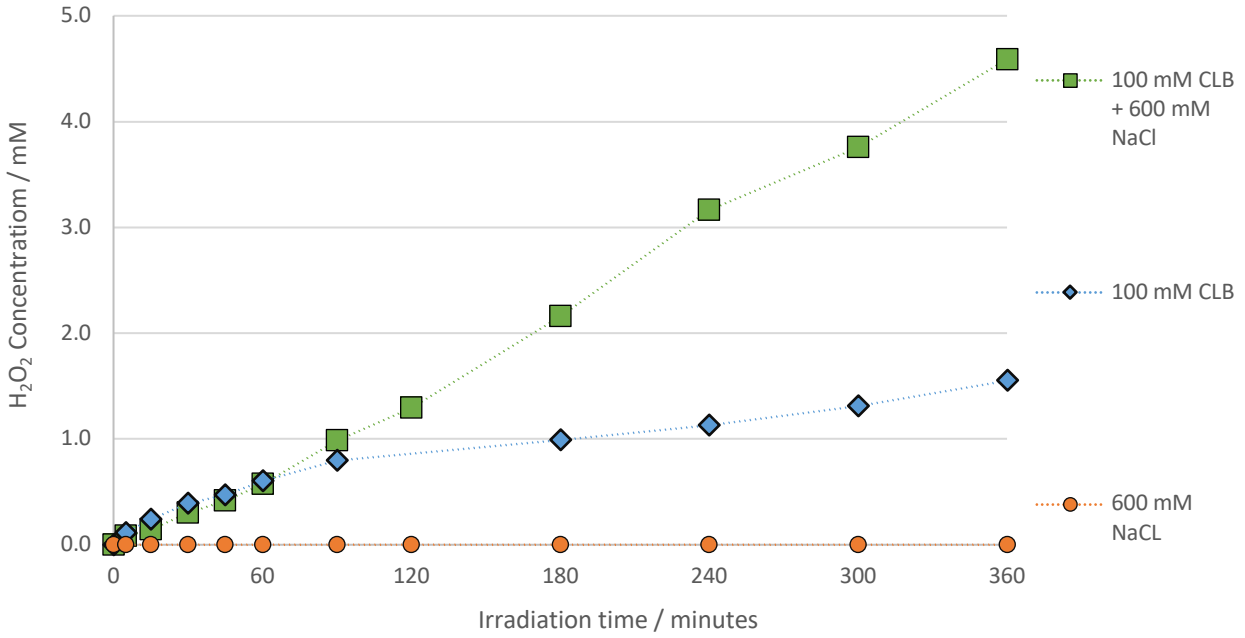



**Figure 21.** The effect of NaCl presence. Experimental conditions: 100 mL of an aqueous solution (UPW); 1.0 g $L^{-1}$ catalyst load (powder); and $\lambda_{max}$ = 412 nm.

One possible factor for the NaCl solution enhancement effect could be the oxidation of $Cl^-$ by photogenerated holes to form chlorine ($Cl_2$) which may happens before the oxidation of water, as shown by equation 16. The $Cl_2$ is in disproportionation equilibrium with hypochlorous acid (HClO), as shown by equation 17, where the quantity of $Cl_2$ and HClO changes with solution pH, being $Cl_2$ a dominant component in acidic solutions below pH 3 [51], and this solution true pH ranges between 4 and 3. Second, when exposed to sunlight, HClO decomposes into $O_2$ and $Cl^-$, as shown by equation 18. As a result, the photocatalytic oxidation of $Cl^-$ in seawater could enhance the photocatalytic generation of $H_2O_2$ in seawater [51].

$$2\,Cl^- + 2\,h^+ \xrightarrow{hv} Cl_2 \qquad \textbf{(16)}$$

$$Cl_2 + H_2O \rightleftharpoons HClO + H^+ + Cl^- \qquad \textbf{(17)}$$

$$2\,HCLO \xrightarrow{hv} O_2 + 2\,H^+ + 2\,Cl^- \qquad \textbf{(18)}$$

The reagents required to evaluate the influence of the main component ions of seawater were then separately added to distinctive solutions of 100 mM cellobiose with 600 mM NaCl. Because seawater has different characteristics and compositions across the world, the worst-case scenario was considered. Thus, these studies were carried out with a greater concentration of these ions than the average in typical seawater [49].

Some of the components, such as KCl and $Na_2SO_4$, appear to have little or no effect on $H_2O_2$ generation (Figure 22). However, $MgCl_2$ and $CaCl_2$ showed a significantly disadvantageous effect. When all of these are combined, the generation of $H_2O_2$ decreases. After 2 hours, the solution containing only 100 mM of cellobiose and 600 mM generated 1.289 mM, whereas the solution containing all of them produced 0.691 mM. This means that after 2 hours, productivity had dropped to half.

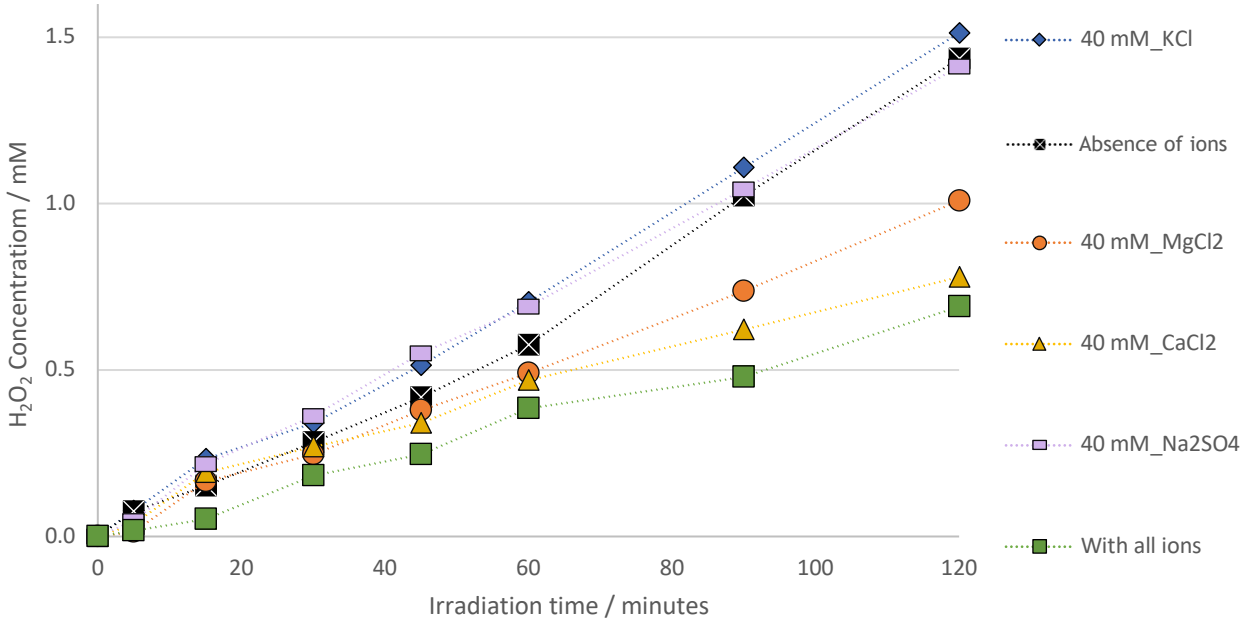



**Figure 22.** Effect of the remaining major constituent ions of seawater. Experimental conditions: 100 mL of an 100 mM aqueous solution (UPW) and 600 mM of NaCl; 1.0 g $L^{-1}$ catalyst load (powder); and $\lambda_{max}$ = 412 nm.

## 4.4 Photocatalytic $H_2O_2$ production using actual seawater

It is certainly possible that several contaminants are present in seawater, but their influence on $H_2O_2$ generation has not been studied. However, because the principal component ions were analyzed in slightly excess, a poorer result with real seawater is not expected to be achieved than with the synthetic combination.

After 3 hours, it generated 0.991 mM using ultrapurified water and 0.900 mM with seawater (Figure 23). Even though production was negatively impacted in comparison with the results

obtained using UPW as a solvent it was still achievable. A reaction using seawater and catalyst was also performed, and the results showed no $H_2O_2$ production, which indicates that any of its components present in the seawater sample can act as a sacrificial agent. Nevertheless, the results proved that even in little concentrations, this system using actual seawater produces $H_2O_2$.

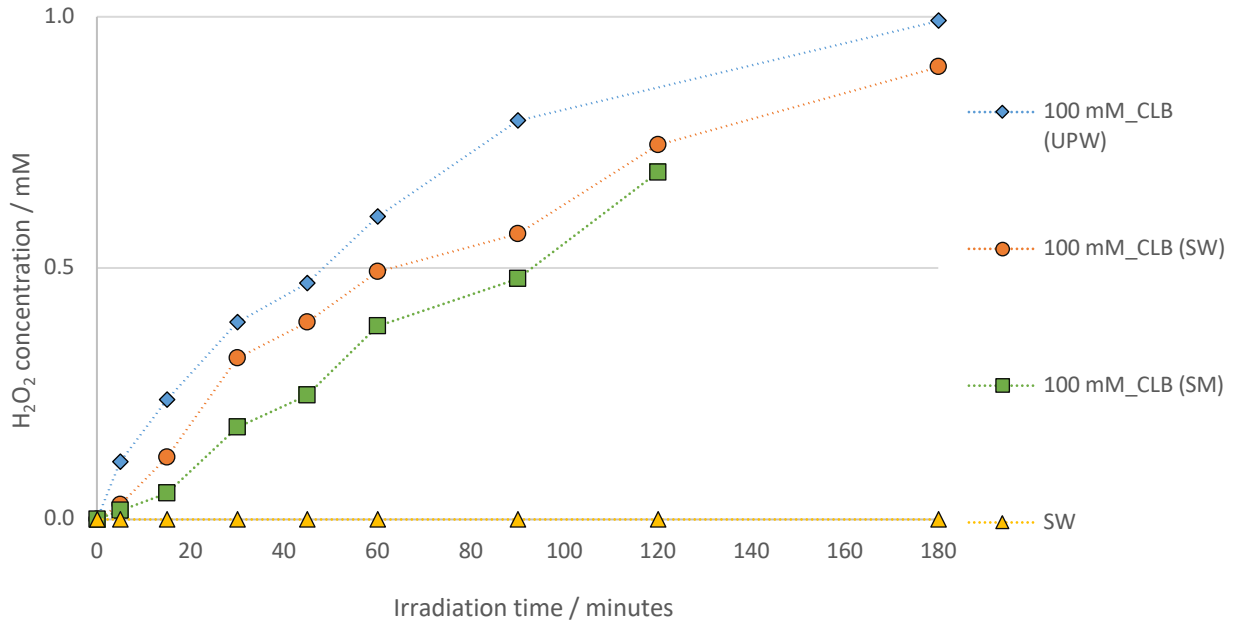



**Figure 23.** The development of $H_2O_2$ concentration in UPW water, the generated synthetic mixture (SM), and actual seawater (SW) are compared. Experimental conditions: 100 mL of an aqueous solution; 1.0 g $L^{-1}$ catalyst load (powder); and $\lambda_{max}$ = 412 nm.

## 4.5 GCN-T immobilized in a polymeric film

### 4.5.1 Photocatalytic $H_2O_2$ production in UPW

As observed in Figure 24, when immobilizing the GCN-T on film, the initial concentration of cellobiose seems to have a negligible effect on $H_2O_2$ generation. After 3 hours of irradiation, 0.241 mM of $H_2O_2$ is produced for a concentration of 20 mM of cellobiose and using 100 mM the $H_2O_2$ production was quite similar (0.278 mM). The initial cellobiose concentration used was fivefold higher, whereas the amount of $H_2O_2$ generated increased ca. 0.15 times.

This is likely related to the unequal distribution of the catalyst in the film. The catalyst amount available to participate in the reaction reduces drastically with the creation of the clusters and the little layer of polymer on top of the powdered catalyst. Since the catalyst, in this case, is in very little amount, the active sites to react are unable to keep up with the extra amount of sacrificial agent available, resulting in a limitation in the formation and release of $H_2O_2$

molecules. As a result, increasing the initial concentration does not have the hoped-for outcome.

By directly comparing the evolution of production from 20 mM solutions, was found that the formation of $H_2O_2$ is much lower. When the catalyst is suspended, a high catalyst area is available to potential the photocatalytic reaction. Because just a part of the solution is in direct contact with the immobilized catalyst, the formation of $H_2O_2$ is more dependent on molecule diffusion and solution agitation. Thus, it is expected slower reaction kinetics with the immobilized catalyst, resulting in less $H_2O_2$ generation for the same irradiation period.

Unfortunately, it was not possible to conduct research on specific film characteristics such as film area, film thickness, dispersion processes, and catalyst application in this present work. Nevertheless, it is expected if the film properties are improved, the process efficiency can increase.

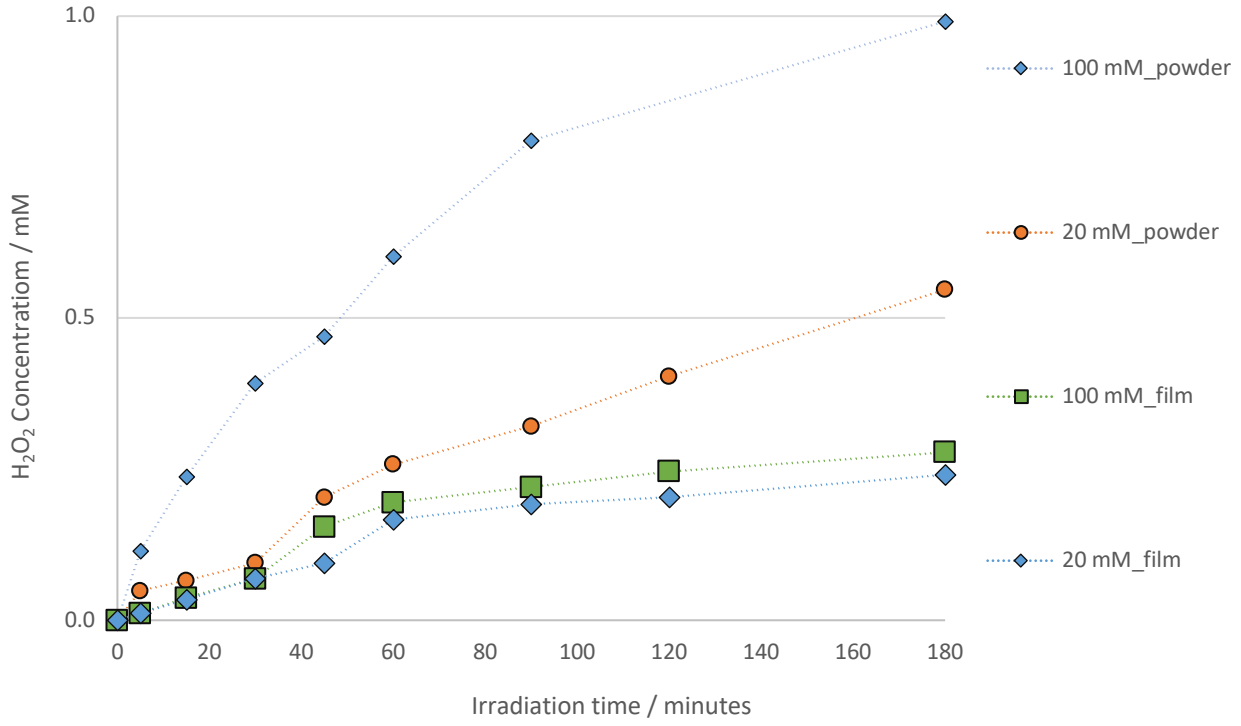



**Figure 24.** $H_2O_2$ concentration evolution using GCN-T immobilized in a polymeric film. Experimental conditions: 100 mL of an aqueous solution of cellobiose (UPW); and $\lambda_{max}$ = 412 nm.

### 4.5.2 Reutilization experiments using the catalyst immobilized in a polymeric film

Although the powdered catalyst enables higher efficiency for $H_2O_2$ generation, it has the disadvantage of having to be separated and cleaned to be reused, which can involve a substantial effort and time-consuming. The immobilization of the catalyst solves this problem,

requiring only a quick washing of the film with clean water. After performing three reactions under the same conditions, the same quantity of $H_2O_2$ was obtained (Figure 25), demonstrating that the film shows high stability under the experimental conditions used. The $H_2O_2$ concentration found after 3 hours of irradiation (Figure 25) differs less than 2.9 % relative error.

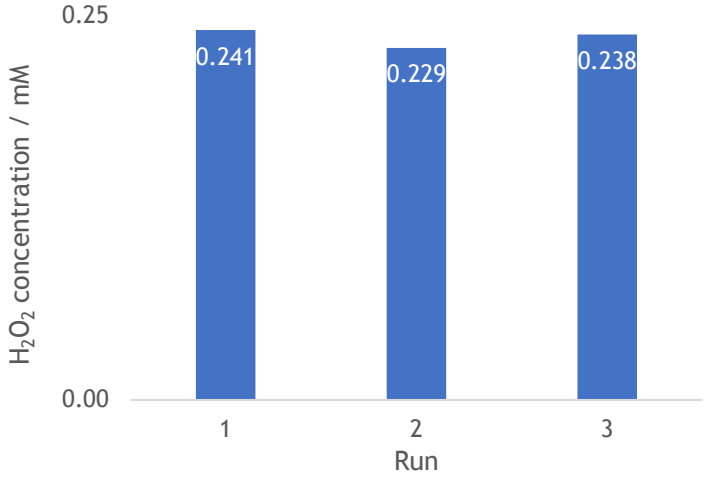



**Figure 25.** $H_2O_2$ concentration after 3 hours of irradiation, using GCN-T immobilized in a polymeric film from 3 distinct reactions. Experimental conditions: 100 mL of an aqueous solution of 20 mM cellobiose (UPW); and $\lambda_{max}$ = 412 nm.

## 4.6 GCN-T immobilized in a 3D printed structure

### 4.6.1 Photocatalytic $H_2O_2$ production in UPW

When the catalyst was immobilized on the cylindrical structure designed by additive manufacturing, the substantially raising in the initial concentration of cellobiose appears to significantly influence $H_2O_2$ production. The photoactive area of the structure is approximately three times higher compared with the flat film (149.66 $cm^2$ and 55.68 $cm^2$, respectively), and while the catalyst does not cover the whole surface area, the distribution is free of agglomeration. With this, a superior performance of this immobilization is predicted. After 3 hours of irradiation, 0.255 mM $H_2O_2$ is formed at a concentration of 20 mM and 0.788 mM at a concentration of 100 mM (Figure 26). The initial cellobiose concentration was raised fivefold, whereas the quantity of $H_2O_2$ produced increased three times. The difference between these similar values in initial solutions of the same concentration is found to be proportional to each other. The prediction has been confirmed, the structure also allows to produce $H_2O_2$, although at a slower rate.

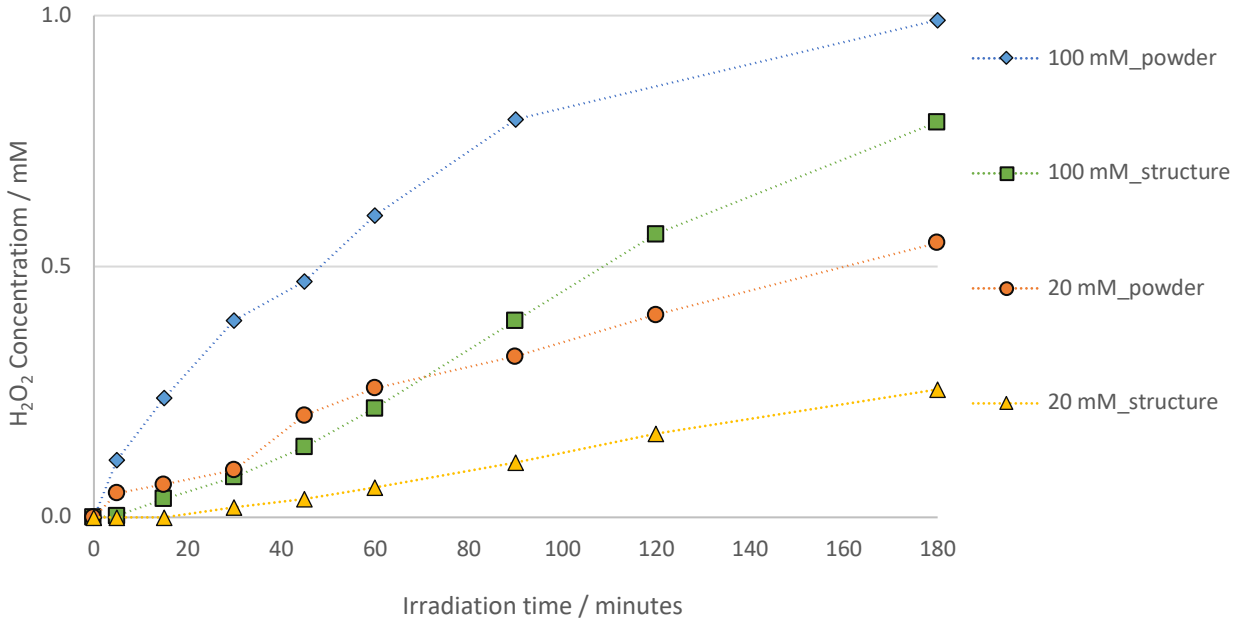



**Figure 26.** Effect of initial concentration of cellobiose (20 mM and 100 mM) using powder and immobilized GCN-T. Experimental conditions: 100 mL of an aqueous solution of cellobiose (UPW); and $\lambda_{max}$ = 412 nm.

### 4.6.2 Reutilization experiments using the 3D printed structure

The same cleaning procedure used in the experiment with the flat film was applied. After performing three reactions under similar conditions, the same quantity of $H_2O_2$ was obtained (Figure 27a), confirming the high stability of the catalyst under the experimental conditions. The $H_2O_2$ concentration found after 3 hours of irradiation in Figure 27 differ by less than 2 % relative error.

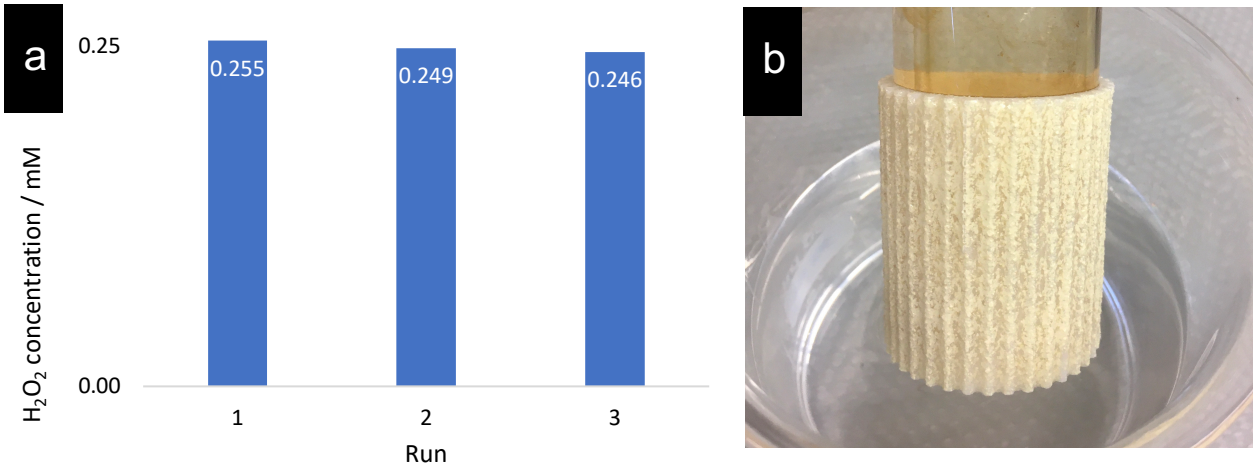



**Figure 27.** a) $H_2O_2$ concentration after 3 hours of irradiation, using GCN-T immobilized in cylindrical structure design by additive manufacturing, from 3 different reactions. Experimental conditions: 100 mL of an aqueous solution of 20 mM cellobiose (UPW); and $\lambda_{max}$ = 412 nm; b) The GCN-T coated structure.

### 4.6.3 Photocatalytic $H_2O_2$ production in actual seawater using immobilized GCN-T

Photocatalytic experiments using the GCN-T immobilized in the cylindrical structure were performed under similar conditions yet using an actual seawater sample. It is found once more that the variation in $H_2O_2$ concentration values derived from initial solutions of the same concentration is proportional to each other (Figure 28). After 3 hours, using a seawater solution with 100 mM and 20 mM initial concentrations of cellobiose, it was produced 0.404 mM and 0.117 mM of $H_2O_2$, respectively. Being compared to 0.788 mM and 0.255 mM $H_2O_2$ formed using initial concentrations of 100 mM and 20 mM of cellobiose in UPW, respectively. This study has proven the efficiency of the immobilized GCN-T using seawater.

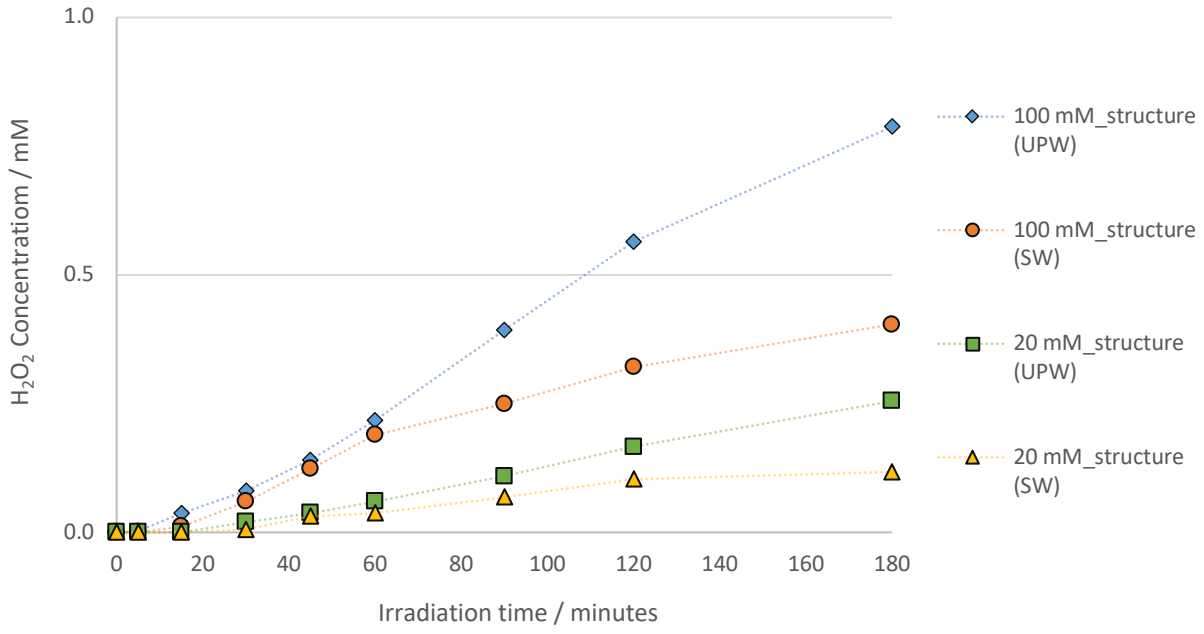



**Figure 28.** Effect of initial concentration of cellobiose (20 mM and 100 mM). Experimental conditions: 100 mL of an aqueous solution of cellobiose using seawater (SW); and $\lambda_{max}$ = 412 nm.

### 4.6.4 3D printed structure reuse using real seawater

The same cleaning process as in the reactions using UPW with the GCN-T immobilized was used. A nearly identical amount of $H_2O_2$ was obtained after three reactions under similar conditions (Figure 29), indicating that the catalyst holds good stability under the testing conditions. Figure 29 shows the $H_2O_2$ concentration after 3 hours of irradiation that differs by less than 4.3 % relative error.

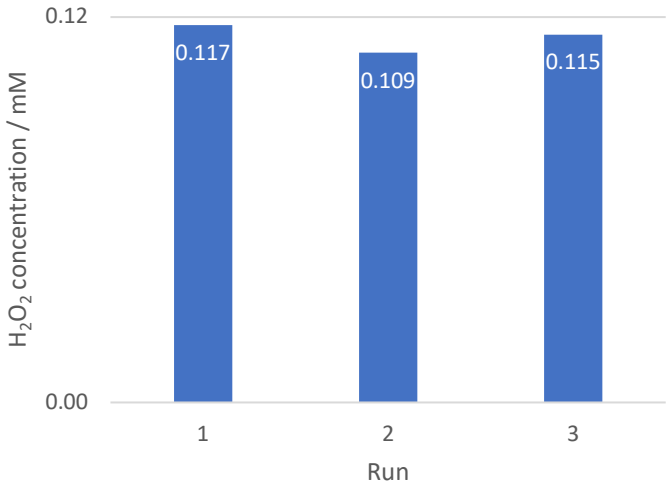



**Figure 29.** $H_2O_2$ concentration after 3 hours of irradiation, using GCN-T immobilized in cylindrical structure design by additive manufacturing, from 3 different reactions. Experimental conditions: 100 mL of an aqueous solution of 20 mM cellobiose using seawater (SW); and $\lambda_{max}$ = 412 nm.

## 4.7 Apparent quantum efficiency

The apparent quantum efficiency (AQE) is a measurement between the photoexcited electrons that allowed the $O_2$ reduction and subsequent $H_2O_2$ production (2 electrons for each $H_2O_2$ molecule) and the quantity of the incident photons on the catalyst, as expressed in equation 19.

$$\mathrm{AQE} = \frac{2 \times \text{number of } \mathrm{H_2O_2} \text{ molecules}}{\text{number of incident photons}} \times 100\,\% = \frac{2 \times n \times N_A \times h \times c}{S \times P \times t \times \lambda} \times 100\,\% \qquad \textbf{(19)}$$

Being $n$ the amount of $H_2O_2$ molecules, $N_A$ the Avogadro constant, $h$ the Plank constant, $c$ the speed of light, $S$ the irradiation area, $P$ the intensity of irradiation light, $t$ the photocatalytic reaction time, and $\lambda$ the wavelength of the monochromatic light [52]. The values used to calculate the AQE of each type of catalyst are shown in Table C1 (supplementary data). The greater the AQE value, the more effective the catalyst.

Figure 30b, shows a comparison between the catalysts in powder form (GCN and GCN-T) and the GCN-T immobilized in the two distinct structures. As displayed, bulk GCN powder material has a significantly low AQE (about 0.002 %) compared with the powder GCN-T catalyst (approximately 0.030 %) under equal experimental reaction conditions. This was already expected since the kinetic formation of $H_2O_2$ was significantly lower compared with the results obtained with the powder GCN-T catalyst (Figure 16).

Comparing the results using powder photocatalysts with the immobilized was observed that even the powder GCN-T material produced high concentrations of $H_2O_2$ under similar experimental conditions in terms of AQE was found small values (Figure 30). This might be explained by the fact that the three separate catalyst systems do not have the same quantity of catalyst available. The quantity of catalyst is not accounted for in the AQE equation, therefore the photocatalytic generation of $H_2O_2$ by the various systems might proportionately correspond to the values of AQE if the same amount of catalyst was available to react in each.

Furthermore, in the case of the immobilized catalyst, the incident irradiance is reduced since it is immobilized in the cooling system and hence further away from the LEDs. Thus, the irradiated surface area of each catalyst particle influences these values. In the case of powdered catalyst, the light constantly excites the entire surface area of each particle, from all angles, in solution. Irradiation reaches the whole surface of the catalyst particles while the particles are agitated. When the catalyst is immobilized, the light excites the same catalyst area, thus only a portion of the surface area of all immobilized particles exposed is irradiated.

Despite the numerous constraints, immobilization systems proved their potential by exhibiting higher AQE values under the experimental conditions used in the present study. Among the photocatalytic systems used, the GCN-T structure revealed a high AQE (0.059 %) followed by GCN-T film (0.055 %), and 0.002 % and 0.030 % when powder catalysts were employed, bulk GCN and GCN-T, respectively.

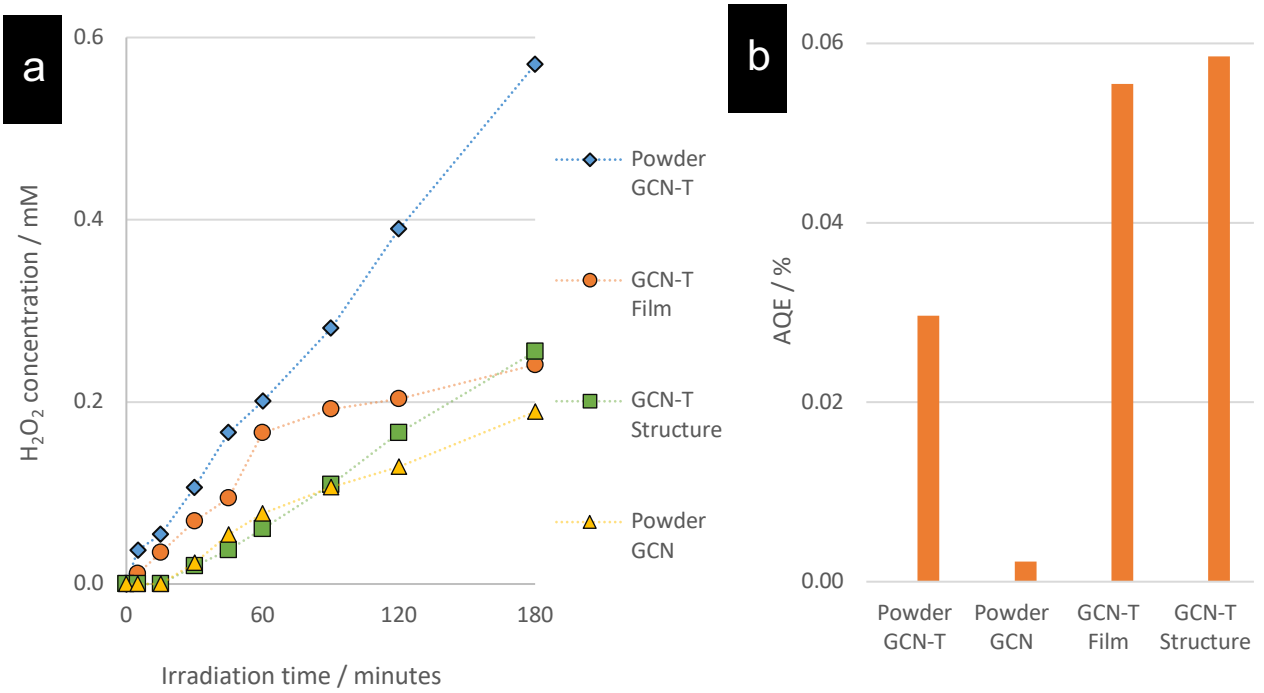



**Figure 30.** $H_2O_2$ concentration evolution using powder bulk, powder GCN-T, GCN-T coated film, and GCN-T coated structure. Experimental conditions: 100 mL of an aqueous solution of 20 mM cellobiose in UPW; and $\lambda_{max}$ = 412 nm.

# 5 Conclusion

In the present work, several operational parameters were investigated in the production of $H_2O_2$ by semiconductor photocatalysis under visible light irradiation.

The study started to evaluate the efficiency of the photocatalytic process for $H_2O_2$ production using various biomass derivatives as sacrificial agents. Among the saccharides tested the cellobiose presented the best efficiency for $H_2O_2$ generation, achieving 0.570 mM using an initial concentration of 20 mM of cellobiose after 3 hours of reaction. Then, the effect of the initial CLB concentration on $H_2O_2$ generation was investigated. Results showed that by increasing the concentration of cellobiose the efficiency of the process was enhanced, *e.g.*, using 5 mM and 100 mM of initial concentration of cellobiose the $H_2O_2$ production after 7.5 hours of irradiation achieved 0.413 mM and 1.848 mM, respectively.

In addition, it was found that cellobiose holds similar performance compared with 2-propanol (a typical model molecule used as a sacrificial agent for $H_2O_2$ production) for at least the first 3 hours of irradiation. The photocatalyst system using GCN-T photocatalyst showed great efficiency for at least 22 hours of reaction, being achieved 4.590 mM of $H_2O_2$ from a 100 mM cellobiose solution. Moreover, this experiment revealed that under the experimental conditions the $H_2O_2$ produced remains stable in solution.

Using simulated seawater (synthetic mixture) the results revealed that the presence of NaCl improved the production of $H_2O_2$, being generated 4.587 mM after 6 hours of irradiation. When all the other major ions commonly present in seawater were added, the process efficiency decreased. Nevertheless, when actual seawater was used in the photocatalytic reactions in presence of 100 mM of cellobiose comparable concentrations values of $H_2O_2$ produced were achieved compared with the results found using ultrapurified water (0.900 mM and 0.991 mM, respectively). This result constitutes a breakthrough in the field of $H_2O_2$ production using photocatalytic systems since seawater could be used as a new source for the generation of sustainable liquid fuels.

Concerning the application of immobilized systems, it was found that supports were efficient for $H_2O_2$ production. Nevertheless, when compared with the suspension system the catalyst immobilized exhibited lower concentration due to the different amount of available area of the GCN-T catalyst in the reaction system. The reutilization tests revealed high stability for both immobilized systems studied. In addition, the use of seawater did not affect the efficiency and stability of photocatalysts, being achieved great stability after 3 cycles.

Overall, this work revealed the possibility of using a metal-free catalyst that produces $H_2O_2$ in a completely sustainable approach using seawater and visible light irradiation while combining

biomass as a sacrificial agent instead of synthesized products. Another main goal achieved was the production of $H_2O_2$ using a system with an immobilized photocatalyst.

# 6 Assessment of the work done

## 6.1 Objectives Achieved

Instead of chemicals fabricated through polluting procedures, biomass was used as a sacrificial agent, and seawater was used to replace potable water. When combined with GCN-T, an air entry, and visible light irradiation, the goal of developing a feasible photocatalytic system that produces $H_2O_2$ in a completely sustainable manner utilizing visible light and a metal-free catalyst is achieved.

To improve the $H_2O_2$ production process, both catalyst immobilization on distinct supports allowed for simple re-use of the catalyst as well as $H_2O_2$ production. The goal of making the same production technique using an immobilized catalyst was accomplished, demonstrating significant potential.

## 6.2 Final Assessment

This study has contributed to the development of a viable photocatalytic system that produces $H_2O_2$ in an entirely sustainable manner by utilizing visible light, a metal-free catalyst, seawater, and biomass. Given the fact that it was a first approach to this technology with these components, the findings are encouraging, yet there is still plenty to learn and improve.

The deviation from the original proposal was essentially non-existent, and the major goals were accomplished. Throughout the course of the project, I was always given the required assistance and was able to get some work experience.

Doing this project was personally fulfilling. I got the opportunity to work on a subject that I am passionate about and to be a member of an outstanding research team.

## 6.3 Limitations and recommendations for future work

Because of the innovative nature of this technique, there is still much to be learned and improved that could not be accomplished or addressed during the development of this work

An attempt was undertaken to gain insight into the mechanism of the cellobiose oxidation process. When executing the various reactions with varied initial cellobiose concentrations (Figure 18), a portion of the samples collected over time was deposited in different vials for High-Performance Liquid Chromatography (HPLC) analysis. However, the findings were inconclusive. This study made it seem that cellobiose concentrations remained stable throughout time. This might be explained by the cellobiose being in excess and the inability to distinguish between what was being consumed. However, if this were true, varied beginning

concentrations would allow the same limited quantity of $H_2O_2$. As a result, the reaction mechanism of photocatalytic oxidation may result in the creation of products with the same retention time, making it impossible to track the consumption of cellobiose by this method. As a result, a thorough investigation of this reaction mechanism is recommended. Not only to track cellobiose, but also to investigate the impact of its byproducts on the generation of $H_2O_2$ and the characteristics of the reaction medium.

Both the film and the structure demonstrate a lot of promise for use in this approach. There is lots of space for improvement. Some of the characteristics to be explored in the film include height, film layer thickness, and ways of spreading the catalyst on the film. In terms of the structure, the characteristics to be investigated may include the form of the structure surface, and the technique of application and dispersion of the catalyst on it.

When $H_2O_2$ is produced using the SM, it was found that the principal component of seawater (NaCl) is favorable. Other main elements appear to be hindering its production. Thus, methods of treating and eliminating only detrimental components might be investigated, focusing on those that enhance $H_2O_2$ production. Another area of innovation that would be to investigate using this approach is the application under continuous mode for $H_2O_2$ production.

# 7 References


1. Affairs, U.N.-D.o.E.a.S. *Do you know all 17 SDGs?* Sustainable Development 2022; Accessed on: 2022/06/03; Available from: https://sdgs.un.org/goals.
2. J., R., J. H., and P. R., *Multi-gas contributors to global climate change*, in *Pew Center on Global Climate Change*. 2003, Massachusetts Institute of Technology.
3. *World Greenhouse Gas Emissions in 2018 (Sector | End Use | Gas)*. Climate Program 2021; Accessed on: 03/15/2022; Available from: https://www.wri.org/data/world-greenhouse-gas-emissions-2018.
4. Vollset, S.E., et al., *Fertility, mortality, migration, and population scenarios for 195 countries and territories from 2017 to 2100: a forecasting analysis for the Global Burden of Disease Study*. The Lancet, 2020. **396**(10258): p. 1285-1306.
5. Statistics, I. *Electric power consumption (kWh per capita)*. 2014; Accessed on: 03/15/2022; Available from: https://data.worldbank.org/indicator/EG.USE.ELEC.KH.PC.
6. Benamor, A., M. Nasser, and M.J. Al-Marri, *Gas Processing Technology-Treatment and Utilization*, in *Encyclopedia of Sustainable Technologies*. 2017. p. 359-387.
7. Ong, W.J., et al., *Graphitic Carbon Nitride (g-C3N4)-Based Photocatalysts for Artificial Photosynthesis and Environmental Remediation: Are We a Step Closer To Achieving Sustainability?* Chem Rev, 2016. **116**(12): p. 7159-329.
8. Sönnichsen, N. *Average annual Brent crude oil price from 1976 to 2022*. Petroleum & Refinery 2022; Accessed on: 06/20/2022; Available from: https://www.statista.com/statistics/262860/uk-brent-crude-oil-price-changes-since-1976/.
9. Kuo, G. *When Fossil Fuels Run Out, What Then?* 2019; Accessed on: 06/01/2022; Available from: https://mahb.stanford.edu/library-item/fossil-fuels-run/.
10. Fathima, A.H. and K. Palanisamy, *Renewable systems and energy storages for hybrid systems*, in *Hybrid-Renewable Energy Systems in Microgrids*. 2018. p. 147-164.
11. Shiraishi, Y., et al., *Highly Selective Production of Hydrogen Peroxide on Graphitic Carbon Nitride (g-C3N4) Photocatalyst Activated by Visible Light*. ACS Catalysis, 2014. **4**(3): p. 774-780.
12. Yan, X.S., W.; Wang, X., *Carbon based electrocatalysts for selective hydrogen peroxide conversion*. New Carbon Materials, 2022. **37**(1).
13. Research, E.M. *Global Hydrogen Peroxide Market Report and Forecast 2021–2026*. 2020; Accessed on: 04/06/2022; Available from: https://www.expertmarketresearch.com/reports/hydrogen-peroxide-market.
14. Disselkamp, R.S., *Can aqueous hydrogen peroxide be used as a stand-alone energy source?* International Journal of Hydrogen Energy, 2010. **35**(3): p. 1049-1053.
15. Kato, S., et al., *Production of hydrogen peroxide as a sustainable solar fuel from water and dioxygen*. Energy & Environmental Science, 2013. **6**(12).
16. Kim, D., et al., *Artificial photosynthesis for sustainable fuel and chemical production*. Angew Chem Int Ed Engl, 2015. **54**(11): p. 3259-66.
17. Fukuzumi, S., *Production of Liquid Solar Fuels and Their Use in Fuel Cells*. Joule, 2017. **1**(4): p. 689-738.

18. Torres-Pinto, A., et al., *Metal-free carbon nitride photocatalysis with in situ hydrogen peroxide generation for the degradation of aromatic compounds*. Applied Catalysis B: Environmental, 2019. **252**: p. 128-137.

19. Lima, M.J., et al., *Graphitic carbon nitride modified by thermal, chemical and mechanical processes as metal-free photocatalyst for the selective synthesis of benzaldehyde from benzyl alcohol*. Journal of Catalysis, 2017. **353**: p. 44-53.

20. Wei, Z., et al., *Efficient visible-light-driven selective oxygen reduction to hydrogen peroxide by oxygen-enriched graphitic carbon nitride polymers*. Energy & Environmental Science, 2018. **11**(9): p. 2581-2589.

21. Torres-Pinto, A., et al., *Recent Strategies for Hydrogen Peroxide Production by Metal-Free Carbon Nitride Photocatalysts*. Catalysts, 2019. **9**(12).

22. Shiklamonov, I. *Water in Crisis: A Guide to the World's Freshwater Resources*. World fresh water resources 1993; Accessed on: 06/05/2022; Peter H. Gleick:[Available from: https://www.usgs.gov/media/images/distribution-water-and-above-earth.

23. Wu, Q., et al., *A metal-free photocatalyst for highly efficient hydrogen peroxide photoproduction in real seawater*. Nat Commun, 2021. **12**(1): p. 483.

24. Song, H., et al., *Photocatalytic Production of Hydrogen Peroxide over Modified Semiconductor Materials: A Minireview*. Topics in Catalysis, 2020. **63**(9-10): p. 895-912.

25. Perea-Moreno, M.-A., E. Samerón-Manzano, and A.-J. Perea-Moreno, *Biomass as Renewable Energy: Worldwide Research Trends*. Sustainability, 2019. **11**(3).

26. Hou, H., X. Zeng, and X. Zhang, *Production of Hydrogen Peroxide by Photocatalytic Processes*. Angew Chem Int Ed Engl, 2020. **59**(40): p. 17356-17376.

27. Tada, H., *Plasmonic Photocatalsyts for Water Splitting and Hydrogen Peroxide Synthesis*. 2020, Open Access.

28. Shiraishi, Y., et al., *Selective Hydrogen Peroxide Formation by Titanium Dioxide Photocatalysis with Benzylic Alcohols and Molecular Oxygen in Water*. ACS Catalysis, 2013. **3**(10): p. 2222-2227.

29. Shiraishi, Y., et al., *Resorcinol-formaldehyde resins as metal-free semiconductor photocatalysts for solar-to-hydrogen peroxide energy conversion*. Nat Mater, 2019. **18**(9): p. 985-993.

30. C., K., B. D., and H. M., *Photocatalytic Production of H2O2 and Organic Peroxides in Aqueous Suspensions of TiO2, ZnO, and Desert Sand*. Environmental Science & Technology, 1988. **22**: p. 798-806.

31. Gogoi, S. and N. Karak, *Solar-Driven Hydrogen Peroxide Production Using Polymer-Supported Carbon Dots as Heterogeneous Catalyst*. Nanomicro Lett, 2017. **9**(4): p. 40.

32. Zuo, G., et al., *Finely dispersed Au nanoparticles on graphitic carbon nitride as highly active photocatalyst for hydrogen peroxide production*. Catalysis Communications, 2019. **123**: p. 69-72.

33. Wang, R., et al., *Energy-level dependent H 2 O 2 production on metal-free, carbon-content tunable carbon nitride photocatalysts*. Journal of Energy Chemistry, 2018. **27**(2): p. 343-350.

34. Zhao, S., et al., *Carbon nanotubes covalent combined with graphitic carbon nitride for photocatalytic hydrogen peroxide production under visible light*. Applied Catalysis B: Environmental, 2018. **224**: p. 725-732.

35. Zhu, Z., et al., *Visible light-driven photocatalytically active g-C3N4 material for enhanced generation of H2O2*. Applied Catalysis B: Environmental, 2018. **232**: p. 19-25.

36. Li, Z., C. Kong, and G. Lu, *Visible Photocatalytic Water Splitting and Photocatalytic Two-Electron Oxygen Formation over Cu- and Fe-Doped g-C3N4*. The Journal of Physical Chemistry C, 2015. **120**(1): p. 56-63.

37. Shiraishi, Y., et al., *Photocatalytic hydrogen peroxide splitting on metal-free powders assisted by phosphoric acid as a stabilizer*. Nat Commun, 2020. **11**(1): p. 3386.

38. Alaghmandfard, A. and K. Ghandi, *A Comprehensive Review of Graphitic Carbon Nitride (g-C3N4)-Metal Oxide-Based Nanocomposites: Potential for Photocatalysis and Sensing*. Nanomaterials (Basel), 2022. **12**(2).

39. Zhang, H., et al., *Switching Oxygen Reduction Pathway by Exfoliating Graphitic Carbon Nitride for Enhanced Photocatalytic Phenol Degradation*. J Phys Chem Lett, 2015. **6**(6): p. 958-63.

40. Cozzi, F., *Immobilization of Organic Catalysts: When, Why, and How*. Advanced Synthesis & Catalysis, 2006. **348**(12-13): p. 1367-1390.

41. Fu, X., et al., *Photocatalytic reforming of biomass: A systematic study of hydrogen evolution from glucose solution*. International Journal of Hydrogen Energy, 2008. **33**(22): p. 6484-6491.

42. Silva, C.G., et al., *Photocatalytic production of hydrogen from methanol and saccharides using carbon nanotube-TiO2 catalysts*. Applied Catalysis B: Environmental, 2015. **178**: p. 82-90.

43. Murugan, A. and R. Selvaraj Mohana, *Environment Friendly g-C3N4-Based Catalysts and Their Recent Strategy in Organic Transformations*. High Energy Chemistry, 2022. **56**(2): p. 73-90.

44. Curriculum Research & Development Group (CRDG), C.o.E. *Practices of Science: Making Simulated Seawater*. Exploring Our Fluid Earth 2022; Accessed on: 06/17/2022; Available from: https://manoa.hawaii.edu/exploringourfluidearth/physical/density-effects/density-temperature-and-salinity/practices-science-making-simulated-seawater.

45. Cotruvo, D.J.A. *Water Desalination Processes and Associated Health and Environmental Issues*. Water Condition & Purification 2005; Accessed on: 17/06/2022; Available from: https://wcponline.com/2005/01/31/water-desalination-processes-associated-health-environmental-issues/.

46. K., K.H.O.Y.M., *Photo-Induced Formation of Peroxide in Saccharides and Related Compounds*. Polymor Journal, 1976. **8**(6): p. 557-563.

47. Pedrosa, M., et al., *Visible-light-induced self-cleaning functional fabrics using graphene oxide/carbon nitride materials*. Applied Surface Science, 2019. **497**.

48. Xu, L., et al., *Pore Structure and Fractal Characteristics of Different Shale Lithofacies in the Dalong Formation in the Western Area of the Lower Yangtze Platform*. Minerals, 2020. **10**(1).

49. Gopakumar, A., et al., *Lignin-Supported Heterogeneous Photocatalyst for the Direct Generation of H2O2 from Seawater*. J Am Chem Soc, 2022. **144**(6): p. 2603-2613.

50. Karagiannis, I.C. and P.G. Soldatos, *Water desalination cost literature: review and assessment*. Desalination, 2008. **223**(1-3): p. 448-456.

51. Mase, K., et al., *Seawater usable for production and consumption of hydrogen peroxide as a solar fuel*. Nat Commun, 2016. **7**: p. 11470.

52. Sampaio, M.J., et al., *Light-driven oxygen evolution from water oxidation with immobilised TiO2 engineered for high performance*. Sci Rep, 2021. **11**(1): p. 21306.

# Appendix A. OceanOptics USB2000 + UV-vis spectrometer calibration curve

Aqueous solutions of $H_2O_2$ were prepared with different concentrations, starting at 0.1 mM and finishing at 3 mM. Then, the coulometric method previously described was applied to each to determine the respective absorbance.

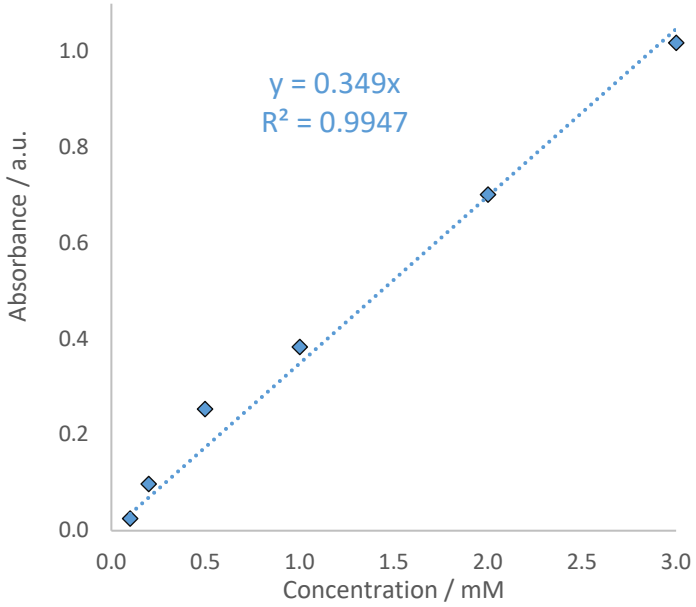



**Figure A1.** Calibration curve of OceanOptics USB2000 + UV-vis spectrometer for determination of $H_2O_2$ concentration.

**Table A1.** Values of the calibration curve of OceanOptics USB2000 + UV-vis spectrometer.

| $H_2O_2$ Concentration / mM | Absorbance / a.u. |
|---|---|
| 0.1 | 0.025 |
| 0.2 | 0.098 |
| 0.5 | 0.254 |
| 1.0 | 0.384 |
| 2.0 | 0.702 |
| 3.0 | 1.018 |

# Appendix B. Preparation of GCN-T

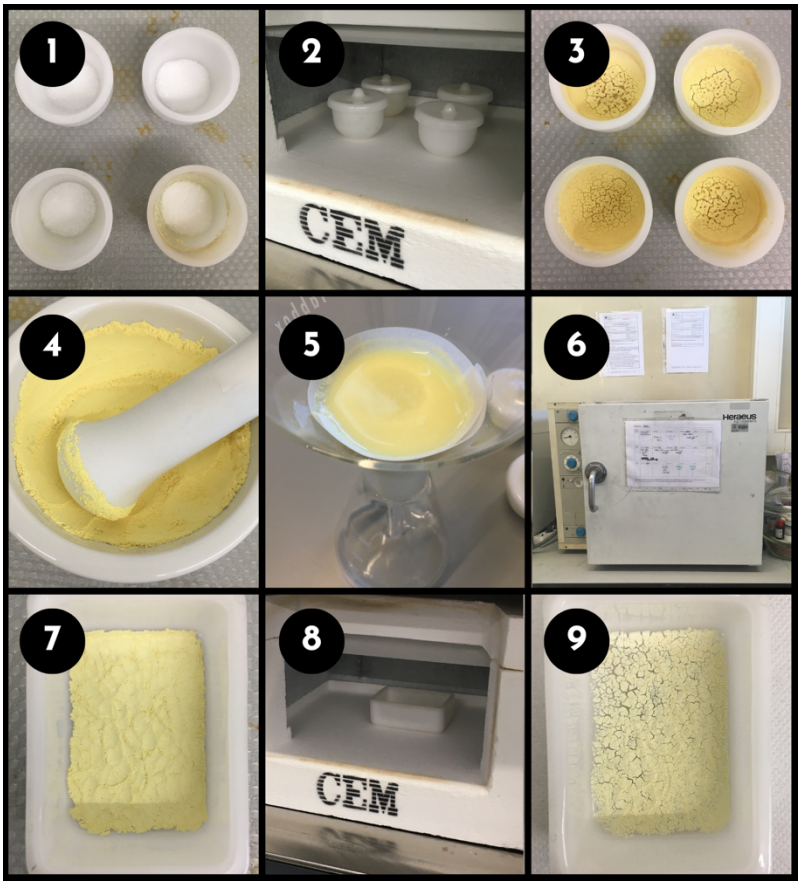



**Figure B1.** Steps to produce the catalyst: 1) dicyandiamide in semi-closed crucible; 2) semi-closed crucibles in the muffle furnace; 3) formation of bulk g-$C_3N_4$; 4) powdering of the bulk; 5) rinsing of the powdered bulk; 6) drying of the bulk on a drying oven; 7) powdered and rinsed bulk in an open crucible; 8) open crucible in the muffle furnace; 9) exfoliated GCN-T.

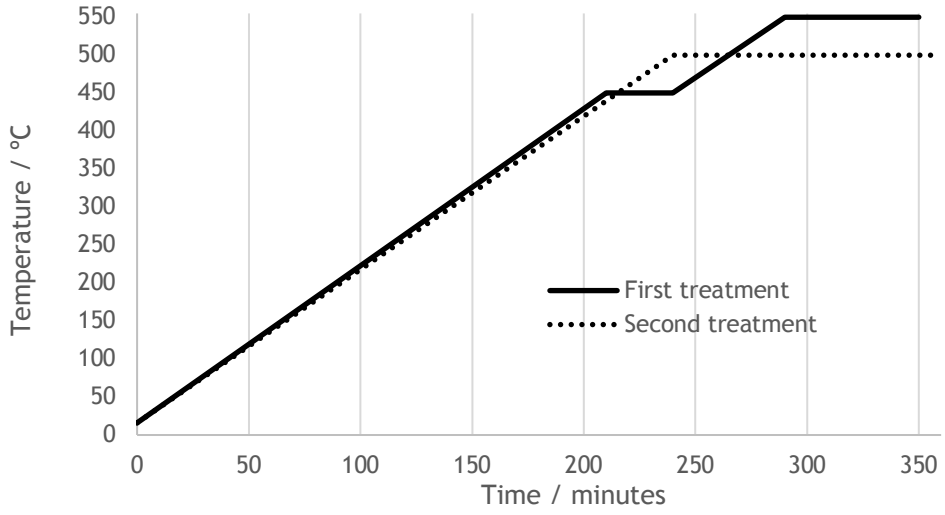



**Figure B2.** Conditions of the thermal treatments applied to produce the catalyst.

# Appendix C. Data for AQE calculations

**Table C1.** Data related to the calculation of AQE of the different systems analyzed.

| | Powder GCN-T | Powder GCN | GCN-T Film | GCN-T Structure |
|---|---|---|---|---|
| ***n* / moles** | $1.41x10^{-04}$ | $1.05x10^{-05}$ | $2.78x10^{-05}$ | $7.88x10^{-05}$ |
| ***S* / cm$^2$** | $1.84x10^{+02}$ | | $5.57x10^{+01}$ | $1.50x10^{+02}$ |
| ***P* / J s$^{-1}$ cm$^{-2}$** | $1.39x10^{-01}$ | | $4.84x10^{-02}$ | |
| ***t* / s** | $1.08x10^{+04}$ | | | |
| ***λ* / m** | $4.12x10^{-07}$ | | | |
| ***h* / J s** | $6.63x10^{-34}$ | | | |
| ***c* / m s$^{-1}$** | $3.00x10^{+08}$ | | | |
| ***$N_A$* / mol$^{-1}$** | $6.02x10^{+23}$ | | | |